geosciences

MDPI

Article

The Taphonomy of Proterozoic Microbial Mats and Implications for Early Diagenetic Silicification

Ashley R. Manning-Berg [1,2,*], R. Seth Wood [1,3], Kenneth H. Williford [4], Andrew D. Czaja [5] and Linda C. Kah [1]

1 Department of Earth and Planetary Sciences, The University of Tennessee, Knoxville, TN 37996, USA; woodr@wustl.edu (R.S.W.); lckah@utk.edu (L.C.K.)
2 Department of Earth, Environmental, and Planetary Sciences, Case Western Reserve University, Cleveland, OH 44106, USA
3 Department of Earth and Planetary Sciences, Washington University, Saint Louis, MO 63130, USA
4 Jet Propulsion Laboratory, California Institute of Technology, Pasadena, CA 91109, USA; Kenneth.H.Williford@jpl.nasa.gov
5 Department of Geology, University of Cincinnati, Cincinnati, OH 45221-0013, USA; andrew.czaja@uc.edu
* Correspondence: Ashley.Manning-Berg@case.edu; Tel.: +1-216-368-3677

Received: 1 December 2018; Accepted: 7 January 2019; Published: 14 January 2019

Abstract: The complex nature of growth and decomposition in microbial mats results in a broad range of microbial preservation. Such taphonomic variability complicates both the description of microbial elements preserved within geologic materials and the potential interpretation of microbial biomarkers. This study uses a taphonomic assessment to explore the preservation of different microbial components within silicified microbial mats of the late Mesoproterozoic (~1.0 Ga) Angmaat Formation, Bylot Supergroup, Baffin Island. The Angmaat Formation consists of unmetamorphosed and essentially undeformed strata that represent intertidal to supratidal deposition within an evaporative microbial flat. Early diagenetic silicification preserved microbial communities across a range of environments, from those episodically exposed to persistently submerged. Here, we present the development of a new methodology involving the use of high-resolution image mosaics to investigate the taphonomy of microfossils preserved in these mats. A taphonomic grade is assigned using a modified classification that accounts for both the taphonomic preservation state (good, fair, poor) of individual microfossils, as well as the degree of compaction of the overall mat. We show that although various taphonomic states occur within each of the silicified mats, the overall taphonomic assessment differentiates between well-preserved mats that are interpreted to have been silicified during active growth, to highly degraded and compacted mats that are interpreted to represent preservation during later stages of biological decomposition. These data indicate that even small changes in the timing of silicification may have substantial implications on our identification of microbial biomarkers and, therefore, our interpretation of early Earth ecosystems.

Keywords: Proterozoic; Taphonomy; Angmaat Formation; microbial mats; silicification

1. Introduction

Microbial mats are highly resilient organosedimentary systems [1–4] in which mat communities are represented by a dynamic and complex ecosystem comprised of photoautotrophic, photoheterotrophic, chemoautotrophic, and heterotrophic populations [4,5]. These microbial communities commonly show a laminated structure that reflects the occurrence of functionally distinct groups of organisms responding to a combination of physical and chemical gradients, such as temperature and light availability, oxygen concentration, pH, and salinity [6]. Although such gradients are most commonly reflected on the

lamina-scale, microscale gradients can occur within individual laminae as well [3,7]. Physiochemical gradients are then reflected in the taphonomy of mat constituents [7–9] that reflect the difference in biologic activity between surficial mats (i.e., regions of active mat accretion that are dominated by photosynthetic production of organic carbon) and buried mats (i.e., subsurface mat communities that are dominated by heterotrophic microbial activity).

An idealized microbial mat can be envisioned as having approximately several layers [4,8–11]. Surficial mat communities are dominated by cyanobacteria. Organisms at the uppermost surface of the mat tend to be associated with dense pigmentation, which provides protection from UV radiation, and with enhanced production of extracellular polymeric substances (EPS) which protects microbes from environmental variability, such as exposure, desiccation, and concomitant changes in salinity [10,11]. Within the cyanobacteria-dominated regions of the mat, oxygenic photosynthesis results in the supersaturation of oxygen and production of gas bubbles [4]. In the lower portions of this zone, microbial decomposition depletes oxygen and light intensities decrease, and photosynthetic purple and green sulfur bacteria dominate [4,10]. Organic matter produced in the photosynthetic upper layers of the microbial mat provide a ready carbon source for heterotrophic organisms at deeper levels of the mat [10]. These deeper mat regions can be dominated by populations of fermenters, sulfate reducers, metal reducing microbes, or methanogens, depending on the composition of pore fluids. With this view in mind, it is easy to envision that the biological and geochemical gradients within a microbial mat should be reflected in both the taphonomy of mat components and, potentially, in chemical signatures associated with preserved materials.

Earth's earliest microfossil assemblages are commonly preserved by silicification [12–14], although substantial controversy exists over the biogenicity of some Archean examples [15–19]. There is, however, little question of biogenicity in most of the Proterozoic samples. Many Proterozoic chert samples contain exceptional but varied morphological preservation of microbial components [20–28]. Because decomposition of cyanobacteria occurs on the time-scale of days to weeks [29], exceptional morphological preservation requires the rapid cessation of heterotrophic activity, and indicates that silicification occurred penecontemporaneously with deposition and prior to the neomorphic recrystallization of mineral phases that can physically destroy organic structures. Determining preservation state is, therefore, critical to our understanding of the extent to which biologic history of materials is accurately preserved. Such understanding is particularly important in light of efforts to develop unique chemical markers, such as the presence of molecular biomarkers [30], the microanalytical identification of carbon sources (cf. [31–35]), and the identification of chemical [36–38] and mineral phases [23,39] associated with microbial activity, to identify microbial activity in both geological and astrobiological samples.

Silicification has been intensively studied in both natural and laboratory systems [40–45], including several experimental studies focused specifically on understanding the role that silicification plays in the preservation of morphological and molecular biosignatures [46–51]. Experimental work supports a silicification model in which microfossils are preserved by a mineralized coating and eventual entombment in silica, similar to that observed in mineralizing spring [46,48,50,52]. By contrast, microfossils preserved in peritidal marine environments typically lack evidence of entombment or mineralized casts and instead have been interpreted to reflect permineralization [53], or complete permeation of preserved microbial structures [54]. Exceptional preservation of primary textures and microbial fabrics, when present, further support this interpretation of silicification of peritidal chert samples. Therefore, questions remain regarding the extent to which data from previous silicification experiments represent the full range of processes of silicification, and whether different mechanisms of silicification may have different potential for preservation of microorganisms and their geochemical signatures.

Here, we describe variations in the preserved morphology of silicified microbial mats of the Angmaat Formation, Bylot Supergroup, northern Baffin Island, in order to understand the range of preservation of ancient microbial mats and the mechanisms that drive differences in preservation.

We describe fundamental differences in the taphonomic response of mat constituents and use high-resolution image mosaics of thin sections as a new way to explore the morphology of these mat fabrics across different spatial scales. Although these methods can be applied to a variety of taphonomic questions, here, taphonomic variation is described across entire thin sections with the goal of understanding the overall taphonomic state prior to performing geochemical analyses on the bulk organic matter.

2. Geologic Setting

2.1. Bylot Supergroup

The Bylot Supergroup contains ~6 km of unmetamorphosed and relatively undeformed sedimentary strata within the fault-bounded Borden basins of the northern Baffin and Bylot islands [54–57]. Three stratigraphic groups, the Eqalulik Group, the Uluksan Group, and the Nunatsiaq Group, record overall basin development (Figure 1). The Eqalulik Group is marked at its base by extrusion of tholeiitic basalt that reflects the initial rifting of the basin. These deposits are overlain by a westward-deepening and fining-upward succession of fluvial to shallow-marine sandstone and marine shale of the Adams Sound and Arctic Bay formations [54], and initiation of restricted marine carbonate deposition in the Iqqittuq Formation [57].

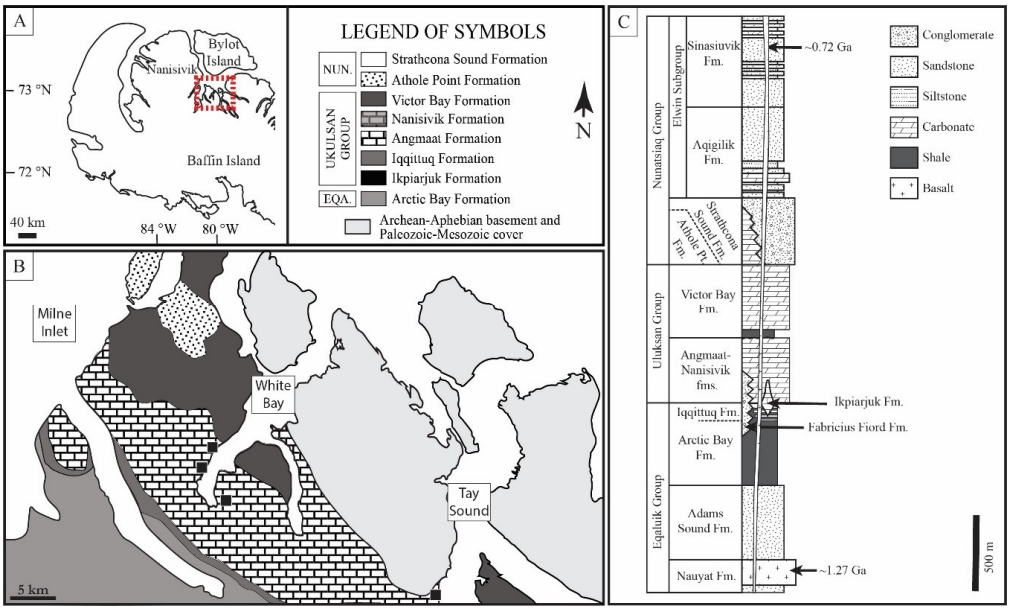

Figure 1. Localities of sample collection from Manning-Berg et al., 2018 [58]. (**A**) Samples were collected during a 1993–1994 field season to northern Baffin Island, Nunavut, Arctic Canada. (**B**) Chert samples were collected from measured stratigraphic sections of the Angmaat Formation at White Bay and Tay Sound. (**C**) The Angmaat Formation represents peritidal carbonate deposition within a restricted platform and is separated from open marine deposits of the coeval Nanisivik Formation by oolitic shoal deposits.

The Eqalulik Group is overlain by the Uluksan Group, which consists of a series of distinct carbonate successions. Initiation of the Uluksan Group is marked by sea-level rise, restriction of terrigenous input into the basin, and the formation of several discrete, deep-water carbonate build-ups associated with fault-derived fluids [59]. Primary deposition of the Uluksan Group is represented by carbonate rocks of the laterally adjacent Angmaat and Nanisivik formations (which, along with the underlying Iqqittuq Formation, were formerly termed the Society Cliffs Formation; [57]), and the overlying Victor Bay Formation [57,59–61]. The Angmaat Formation is represented by a broad microbial flat bounded to the west by an oolitic shoal. Periodic subaerial exposure of the oolitic

shoal resulted in restriction and evaporation of associated nearshore environments that are dominated by microbial dolostone, sea floor precipitates [62], and abundant early diagenetic chert [55,63,64]. Northwest of the oolitic shoal, offshore deposits consist predominantly of finely laminated microbial dolostone and are referred to as the Nanisivik Formation [57]. The Nanisivik contains a large Mississippi-Valley-Type (MVT) deposit [65]. Fluid inclusion data from the carbonate host materials provide a maximum temperature of 130 °C for the basin [65]. MVT deposits are not found in the Angmaat Formation where our samples were collected. The upper Uluksan Group is represented by carbonate ramp [66] and offshore reef [67] deposits of the Victor Bay Formation. These deposits record evidence of tectonic reactivation of the Bylot Basin [60], ultimately leading to thick, lithologically variable sandstone deposits of the Nunatsiaq Group.

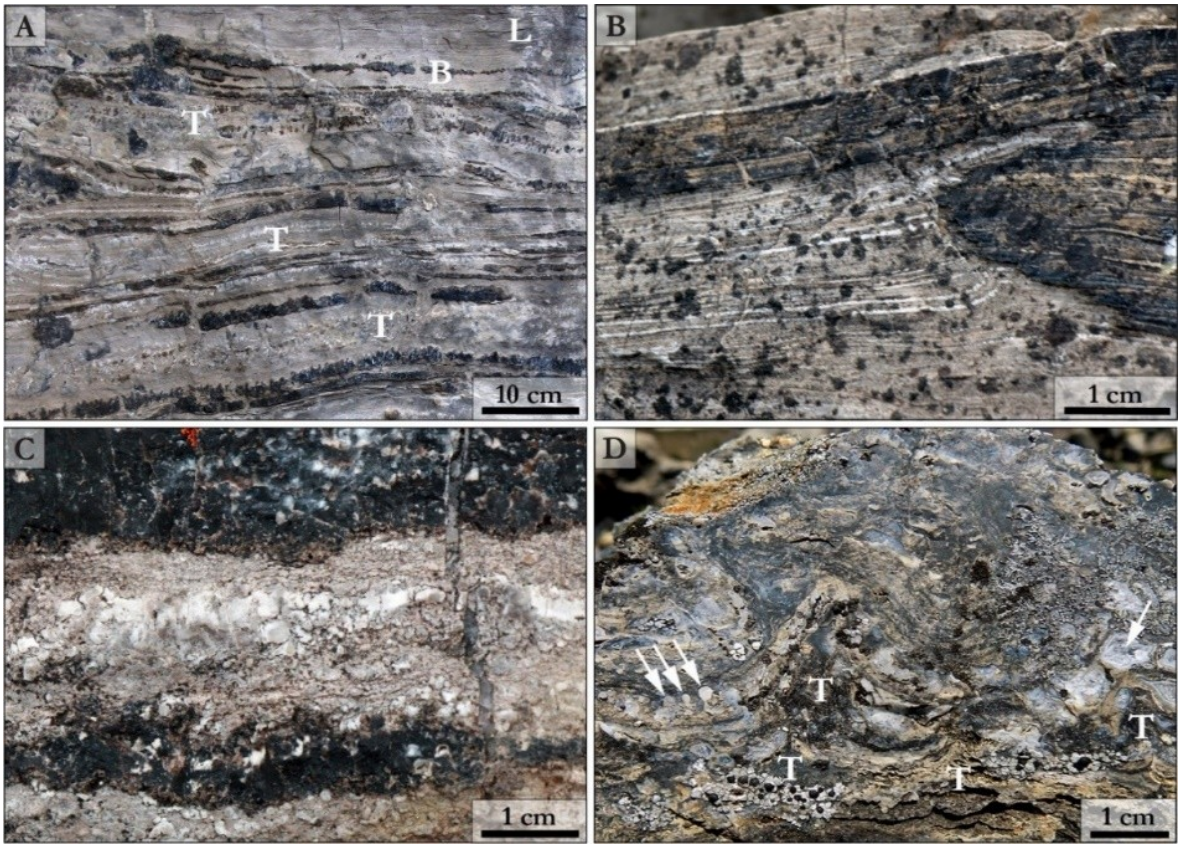

Figure 2. Early diagenetic black chert in outcrop. (**A**) Early diagenetic chert occurs in lenses and beds, and mimic primary tufted [T], blebby [B], and laminated [L] bedding. (**B**) Black chert nodule preserving primary laminated fabric composed of mm-scale alternation of microbial carbonate (grey) and detrital micrite (white). (**C**) Black chert nodules preserving primary blebby fabric composed of microbial carbonate (grey) with mm-scale patches of detrital micrite (white). (**D**) Black chert nodule preserving primary tufted [T] microbial fabrics. Tufted fabric results from the vertical orientation of filamentous microbes, and is characterized by the presence of numerous constructional voids (arrows) that are commonly filled with multiple generations of chalcedony (cf. Knoll et al., 2013) [63].

The age of the Bylot supergroup is broadly constrained to within the late Mesoproterozoic era. Tholeiitic basalts at the base of the Eqalulik Group provide a maximum depositional age of 1.270 ± 0.04 Ga, indicating their emplacement as part of the widespread Mackenzie igneous event [68]. Re-Os dating performed on shale of the Arctic Bay Formation (upper Uluksan Group) and the Victor Bay formation (upper Uluksan Group) yield ages of 1.048 ± 0.012 Ga and 1.046 ± 0.016 Ga, respectively [69], confirming a late Mesoproterozoic age for carbonate-bearing strata of the Uluksan Group that has previously been inferred from chemostratigraphic analysis [56,70]. Although the age of the uppermost

Nunatsiaq Group is poorly constrained, crosscutting dikes that were part of the ~723 Ma Franklin Igneous Event [71] indicate that deposition ended prior to the latter Neoproterozoic era.

2.2. Angmaat Formation Chert

Chert is common in the Angmaat Formation, although it occurs almost exclusively within non-oolitic facies. Black chert deposits are interpreted to be primarily of early diagenetic origin based on ubiquitous microfossil preservation [55,63,72]. Black chert occurs as cm-scale lenses and semi-continuous beds up to 10 cm in thickness that conform to bedding planes [54,55,64], and often reflect the morphology of primary sedimentary textures (Figure 2). By contrast, late diagenetic chert is represented by gray to yellow laminated nodules that characteristically cross-cut bedding (Figure 3).

Figure 3. Late diagenetic chert nodules. (**A**–**C**) By contrast to fabric-retentive early diagenetic chert lenses, late diagenetic chert commonly occurs as concentrically layered, ellipsoidal nodules that cross-cut primary bedding features.

2.3. Microbial Assemblages of the Angmaat Formation

Microbial mat communities of the Angmaat chert are preserved across a range of peritidal environments, wherein subaqueous subtidal environments and lower intertidal environments are dominated by filamentous communities, and more frequently exposed intertidal to supratidal environments are characterized by more abundant coccoidal populations and low-diversity filamentous communities [55,63]. Mat-building and mat-dwelling microbial communities are recorded in four distinct microfossil assemblages [63]. Preserved sheaths represent the filamentous mat-building communities. Small-diameter (6–12 μm) filaments have been interpreted as the extracellular polysaccharide sheaths of *Lyngbya*- or *Phormidium*-type cyanobacteria and classified as *Siphonophycus* sp. [55,56,72]. Filamentous sheaths of larger diameter (20–50 μm) have been assigned to *Eomicrocoleus* sp. (cf. [27]) and interpreted to be analogous to the extant cyanobacteria *Microcoleus chthonoplastes* [63]. Coccoidal populations occur as small mat-dwelling populations, and occasionally as primary mat-builders. Preserved coccoids are varied in their composition [63] but consist predominantly of populations of *Gloeocapsid*-like cyanobacterial assigned to *Eogloeocapsa* sp. [73], which consists of multiple coccoids floating within a single external envelope and simple, undefined coccoidal populations assigned to *Myxococcoides* sp. Additional coccoidal populations can be assigned to *Eoentophysalis* sp., *Gloeodiniopsis* sp., and *Polybessurus* sp. [74], all of which have been compared to modern cyanobacteria [63]. Eukaryotic algae, such as the red alga *Bangiomorpha pubescens* [75], also occur in several samples.

3. Methods

Traditional light microscopy was used to investigate the microbial mat fabrics and individual microfossils preserved in the Angmaat Formation. An Olympus B60 transmitted light microscope was used to describe the fabrics of the microbial mats, and to perform a preliminary taphonomic assessment of individual microfossils. Later analyses used image mosaics for taphonomic assessment (see Taphonomic Techniques below). A first-order assessment of the preservation of organic material was then conducted using Raman spectroscopy. Raman spectroscopy was performed using a Horiba T64000 Raman microscope at the University of Cincinnati using a 50x long working distance objective (N.A. = 0.50) and a 458 nm excitation laser. The laser power at the sample for each analysis was

~9 mW. Each spectrum was integrated for 30 s to achieve an optimal signal-to-noise ratio. Prior to each analysis, the Raman microscope was calibrated using a silicon chip. For all spectra, Raman index of preservation (RIP) values [76], which are a measurement of thermal maturity, were calculated using the equation RIP = 7.6866*(α/γ) [77], where α and γ are integrated areas of each spectrum between 1100 and 1300 cm^{-1}, and between 1300 cm^{-1} and 1370 cm^{-1}, respectively [76].

4. Taphonomic Techniques

4.1. Taphonomic Classification

Taphonomic studies seek to understand how organic remains are incorporated into the rock record [78]. Taphonomic studies are used to inform biases within the fossil record, to provide constraints for paleoecologic, biostratigraphic, and evolution studies, and to understand differential preservation of organisms within fossil assemblages [78]. Taphonomic schemes are built on systematic observations that are used to create descriptive categories into which organisms are categorized [29,79], and great care is taken into creating descriptions to ensure that data are reproducible.

The classification scheme used to assess individual microfossils is modified from the taphonomic grading scale developed by Bartley [29]. This taphonomic scale was developed using actualistic taphonomy experiments to specifically describe changes to cyanobacteria during decomposition. These taphonomic stages broadly follow divisions outlined by Behrensmeyer [79] that represent stages of decomposition that range from immediately post-mortem (i.e., containing evidence of rapidly degrading tissues), to nearly unrecognizable materials.

The grading scheme developed by Bartley [29] focused on changes to cell morphology, trichome articulation, sheath morphology, and terminal cell morphology. These characters were selected based on observations of microfossil populations made by Golubic and Hofmann [80], Oehler [81], Hofmann [82], Knoll and Golubic [83], and Knoll and Barghoorn [84]. Five grades were described by Bartley [29] for each character, and one hundred filaments were scored for each character using a light microscope. Of these characteristics, however, sheath morphology is the primary character that can be applied to silicified microfossils preserved in the Angmaat Formation. Preferential preservation of sheaths relative to cellular material is common in both modern [29,85] and ancient [80,82] assemblages. In the Angmaat chert, preservation of individual trichomes, in or out of sheaths, is exceedingly rare. Most of the cell morphology observed in the Angmaat Formation mats would therefore be given a grade of 5 in the taphonomic scheme defined by Bartley [29], which included morphological detail of cellular trichomes.

To adequately describe the preserved microbial mats of the Angmaat Formation samples, we applied taphonomic grading schemes at two different scales, where the mesoscale taphonomy, defined as the scale of a thin section, represents the overall taphonomy of a preserved microbial mat; and the microscale taphonomy, defined as the taphonomy based on assessment of individual microfossils. At both scales, we used a three-tiered taphonomic grading scheme of "good", "fair", and "poor". A three-tiered grading scheme is commonly used in taphonomic assessments because it allows an entire sample to be easily visualized on ternary taphograms [86]. In cases where organic matter has degraded to the point that the original morphologic features were not able to be recognized, the percent area of unrecognizable organic matter was determined using the threshold feature in ImageJ. The unrecognizable, homogenized organic matter was generally dark brown or black. These areas were highlighted in ImageJ using a mask created via the selection of these dark pixels. The threshold was then refined by focusing on multiple areas of the mosaic to ensure that only the unrecognized organic matter was selected by the threshold. Using the Measure tool under the Analyze tab, the software performed a percent area calculation, which represents the percent area of the mosaic that was covered by the selected threshold.

At the mesoscale, the prominent taphonomic changes are reflected in a loss of structure driven by compaction of the microbial mat. The taphonomic assessment scheme described in

Manning-Berg et al. [58] was used to perform this assessment and is summarized here. Mesoscale fabrics were classified as "good", "fair", or "poor", based on visual inspection of the thin sections (Figure 4). Thin sections classified as "good" typically contain microfossils that are readily visible. Lamina thickness is often irregular in these samples, which is attributed to differential growth and decomposition within the microbial mat, and laminae frequently contain chalcedony-lined voids that reflect constructional voids [64]—interpreted as gas bubbles (cf. [63])—within the microbial mat. By contrast, mesoscale fabrics defined as "fair" contained obviously different concentrations of carbonaceous material. Most of the microfossils observed were concentrated in isolated laminae, and individual microfossils could sometimes be identified. Finally, mesoscale fabrics defined as "poor" were typified by dense color that obscures lamina structure, homogenization of organic matter, and an absence of readily identifiable microfossils. When samples were so strongly pigmented that they appeared nearly opaque in thin sections, they were categorized as "unrecognizable".

At the microscale, taphonomic grades were used to describe both filamentous sheaths and coccoidal microfossils. Filamentous microfossils with pristine sheath preservation that exhibited no evidence of compaction, were classified as a taphonomic grade of "good". Coccoidal microfossils classified as "good" commonly preserved both an outer sheath and a rounded cell wall within the sheath (Figure 5). A grade of "fair" was given to filamentous microfossils that showed signs of compaction. Commonly, these fossils had collapsed or folded sheaths that included tearing or bulging. In coccoidal organisms, a grade of "fair" was indicated by collapse of the cell wall inside the outer sheath (Figure 5). Finally, a grade of "poor" was given to filamentous microfossils that had been heavily distorted by compaction, had lost the morphology of the sheath, or those fossils in which the organic matter was homogenized, and no distinct fossils were recognizable.

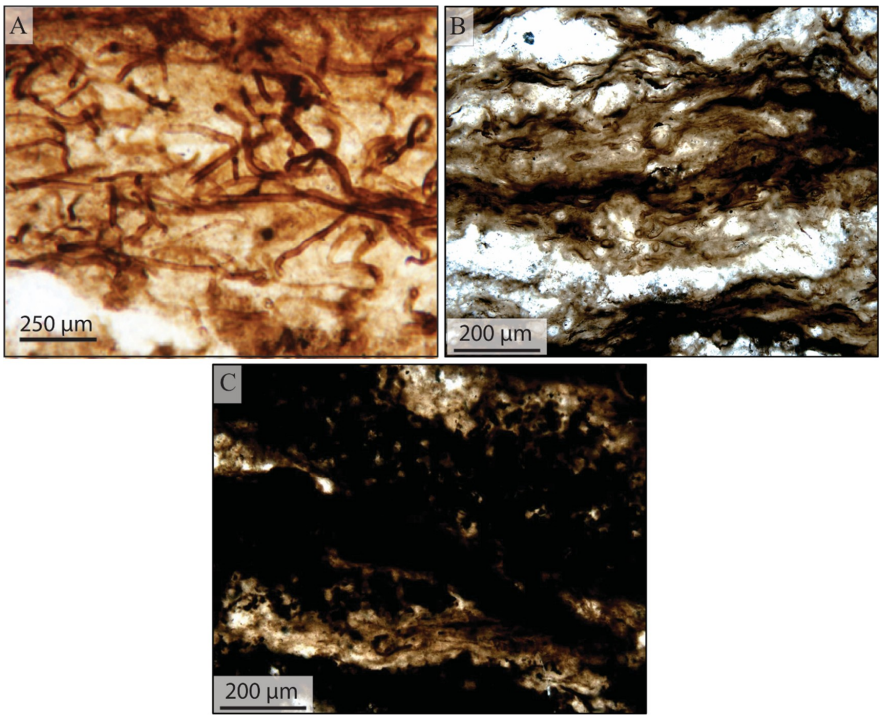

Figure 4. Visual interpretation of overall mat taphonomy. Overall mat taphonomy was determined based on mesoscale petrographic observation. (**A**) Mats with abundant visible microfossils were classified as "good". (**B**) Mat fabrics with clear microbial lamination, but indistinct preservation of individual microbes, were classified as "fair". (**C**) Mat fabrics dominated by largely opaque organic matter, with no visible microfossils present, were classified as "poor". Assessment of individual microfossils within these assemblages was then used to explore the potential variability of mat fabrics. This figure was originally published in Manning-Berg et al. (2018) [58].

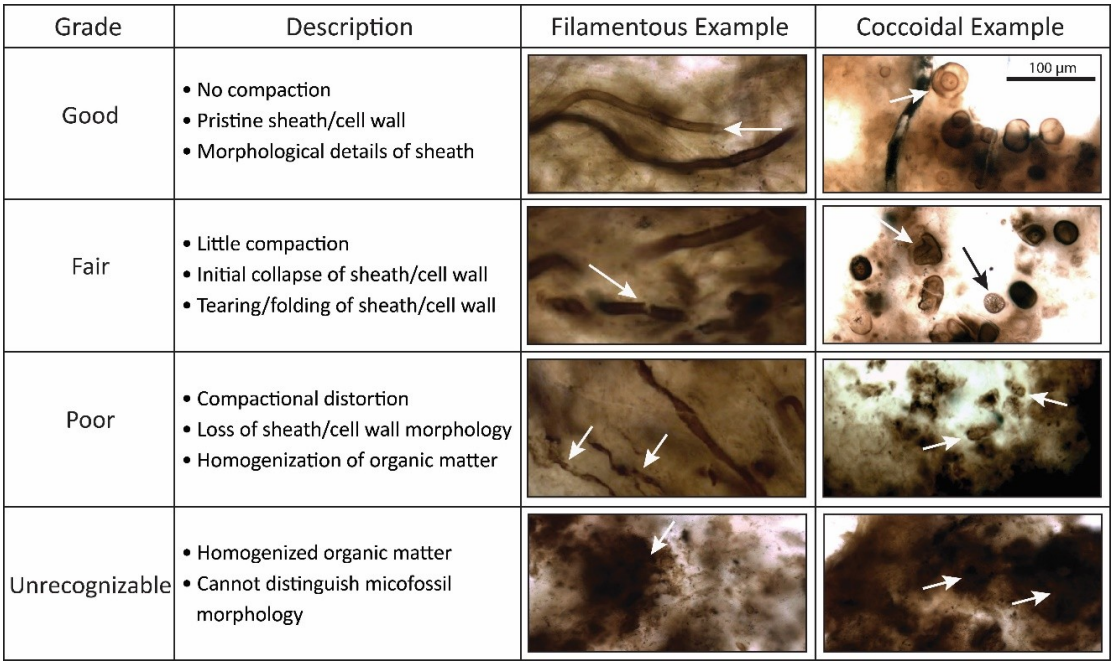

Figure 5. Taphonomic grading of individual microfossils. Classification of "good", "fair", and "poor" were assigned to individual microfossils. These grades were determined based on the compaction of the microfossil, how pristine the sheath or cell wall appeared (i.e., whether it was torn or collapsed). A subcategory of "poor" was used for samples that were too darkly pigmented or where the organic matter was too homogenized to determine whether the microfossil had been filamentous or coccoidal. These samples were labelled as "unrecognizable". This figure was originally published in Manning-Berg et al. (2018) [58].

4.2. Taphonomic Analysis Using Traditional Point Counting

Individual microfossils were first scored using traditional point-counting techniques [87,88]. To assess the taphonomy of individual microbial mat samples, 600 microfossils were counted from each sample when possible [58]. A sample size of 600 microfossils provides a 95% confidence level with a 4% confidence interval (calculated using an online sample size calculator [89]). Obtaining 600 counts, however, was not always feasible. Smaller sample sizes, such as those closer to 150 microfossils, have a 95% confidence level with an 8% confidence interval. Results using traditional point-counting techniques, despite the inherent subjectiveness in defining taphonomic categories, generally fell within 5% when comparing counts performed on the same thin section on different days, and when comparing counts performed by different people.

The traditional point-count method technique and conclusions are outlined in Manning-Berg et al. [58], which concluded that the method was time-consuming and it was often difficult to obtain the 600 counts desired in a single sitting, which introduced the risk of miscounting microfossils [58]. Identification of a single microfossil under the ocular cross-hairs frequently required adjustment of the focal plane to see the microfossil in its entirety, making it difficult to maintain a uniform focal plane through the investigation. Finally, a traditional point-count method failed to accurately produce a representative picture of the overall microbial mat fabric and could not capture variation within a microbial mat, such as the spatially variable occurrence or preservation of different mat constituents.

4.3. Taphonomic Analysis Using Image Mosaics

To alleviate difficulties imparted by traditional point-counting, we developed a method of taphonomic assessment using image mosaics. Image mosaics were produced on a Leica DFC400 camera attached to a Leica DM6000B microscope in the Astrobiogeochemistry Laboratory (abcLab) at NASA's Jet Propulsion Laboratory. The method for creating these images is outlined in Manning-Berg et al. [58].

One of these image mosaics has been uploaded to the GigaPan website and can be viewed by the public [90].

Quadrat Sampling within Image Mosaics

Because the spatial variability and complexity of microbial mats is not readily represented by traditional point-counting techniques, we sought to describe the mat taphonomy in a way that allowed a more detailed view of the overall mat fabric. Quadrat sampling is a technique commonly used in ecological studies to produce an unbiased assessment of populations [91–93]. Specifically, quadrat sampling involves dividing the study area into discrete regions and collecting data on all components within single or multiple quadrats. Such sampling permits investigation of the common or visually obvious components (e.g., here, either the mat building constituents or the most easily recognized components) as well as the rare components of the system.

Because individual image mosaics, which could exceed 2 GB file sizes, are unwieldy for most imaging software, mosaics were split into 25 partitions using the photo editing software Gimp 2.8 (www.gimp.org). Each partition was of equal size—20% of the length of the image and 20% of the width of the image—and represented 4% of the total image. Because images varied in size, a percentage value was used to define the size of a quadrat instead of using a pixel count. Partitions were then saved as discrete tagged image file format (TIFF) files to prevent image compression. Each partition was then opened in Adobe Photoshop and divided into 64 quadrats by overlaying an 8 × 8 grid (Figure 6) using the GuideGuide extension (http://guideguide.me). This method produced a total of 1600 quadrats per thin section, with an average area of 0.0625%, the area of an individual quadrat.

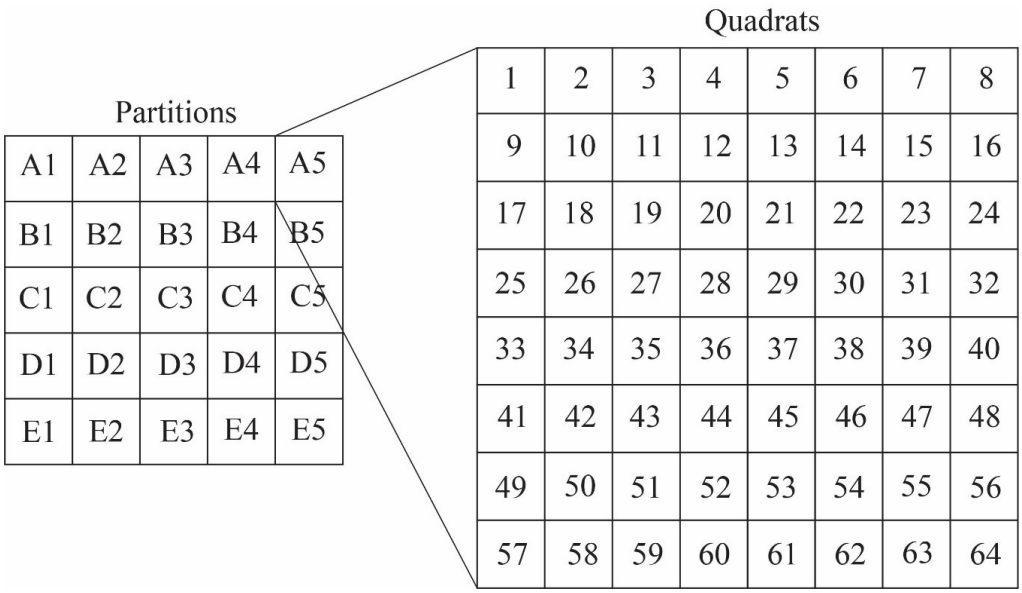

Figure 6. Development of the quadrat system for measuring taphonomy from Gigapan mosaics. Each mosaic was first divided into 25 partitions (A1–E5), and each partition was divided into 64 quadrats (1–64). For each partition, a random number generator in Microsoft Excel was used to determine which quadrat would be used in the taphonomic assessment, with a single quadrat chosen from each partition. Additional quadrats were assigned to increase the number of microfossil counts. Such analysis gives a random assessment of the entire thin section, although the technique could be modified to assess single laminae (e.g., assessment of quadrats from a horizontal row), or a cross-section of the preserved mat (e.g., assessment of quadrats from a vertical column).

A sampling template, created in Microsoft Excel, was used to determine which quadrats would be analyzed and to track results of taphonomic assessment. Within this file, a random number generator provided 25 values that corresponded to a single quadrat in each of the partitions. Taphonomic

assessment of these 25 quadrats provided a random assessment of the entire thin section. For each quadrat, the taphonomic state of every microfossil was assessed. Microfossils were noted as being a filament or coccoid, and assigned an assessment of "good", "fair", or "poor". If needed, this process could be repeated, providing assessment of a second or third quadrat in each partition.

This method of quadrat assessment expands the capabilities of the taphonomic assessment. For instance, addition of secondary or tertiary assessment rounds permitted an evaluation of variability—with low total counts, a single quadrant with extremely well-preserved microfossils can skew the assessment of the entire thin section toward better preservation. A greater number of counts therefore provides an assessment of both individual quadrats (i.e., the spatial variability of preservation) and the preservation of microbial mats as a whole. Assessment of individual quadrats continued until at least 600 microfossils were assessed. Once the goal of counting 600 individual microfossils was reached, the assessment continued until that quadrat was completed.

5. Results

5.1. Mesoscale Taphonomic Patterns

5.1.1. Filamentous Constituents

Two species of filamentous organisms represent the dominant mat-forming constituents within Angmaat chert (Figure 7). Small-diameter (6–12 μm) filament sheaths assigned to *Siphonophycus* sp. are robust and thick-walled and, when well-preserved, occur as tightly woven horizontal mats and as vertical tufts of filaments that outline constructional voids within the mat. These simple forms rarely show evidence of either sheath degradation or compaction. Instead, the primary taphonomic pathway appears to be the gradual loss of coloration, which ultimately inhibits identification of distinct sheaths. The progressive loss of coloration from *Siphonophycus*-dominated regions correlated with light-colored regions of the laminated mats at the mesoscale (Figure 8). By contrast, large-diameter (20–60 μm) filamentous sheaths assigned to *Eomicrocoleus* sp. consist of heavily colored, thin-walled sheaths. *Eomicrocoleus* occurs both as sparse constituents within *Siphonphycus*-dominated mat regions, or as a primary mat component interlaminated with *Siphonophycus*-dominated regions. *Eomicrocoleus*-dominated laminae undergo substantial compaction prior to any visible taphonomic alteration of *Siphonophycus*-dominated regions, resulting in interlamination of thick, lightly colored regions (where sparse sheaths of *Eomicrocoleus* sp. remain relatively undeformed) and thin, heavily pigmented laminae composed of compacted sheaths of *Eomicrocoleus* sp.

5.1.2. Coccoidal Constituents

Several coccoidal species are present in the Angmaat Formation mats. Thin-walled, ~10 μm sized coccoids identified as *Myxococcoides* sp. occur in isolated pockets within filamentous mats. Such pockets tend to be well-preserved, and maintain a circular to oval shape. Coccoid-dominated mats within the Angmaat Formation are commonly dominated by *Eogloeocapsa* sp. [63]. Well-preserved examples have 2–4 cells preserved within a single external envelope. Taphonomically "fair" *Eogloeocapsa* sp. typically preserve a couple of cells within a remnant of the external envelope, or cells preserved just outside of a ruptured envelope. Organisms with a thick envelope surrounding a cell wall, or dark centers (Figure 8), likely the remnant organic matter from a collapsed cell wall [29,94], belong to the taxa *Gloeodiniopsis* sp. Well-preserved *Gloeodiniopsis* sp. are circular to oval in shape, with a dark circle at the center of the envelope. When compacted, these fossils are arranged in layers and lose their round shape with the discrete envelope and dark center pattern. In a poor section of the mat, discrete individual fossils cannot be identified, and their shape is lost (Figure 9). Coccoidal mats contain a lot of lightly-pigmented, structureless regions that surround them; these regions are interpreted as EPS. Within compacted mat fabrics, *Eogloecapsa* behave similarly to Gloeodiniopsis and compact into layers as the envelopes and cells become more oval in shape. Microfossils are more compacted, and

individual cells or envelopes are not identifiable in mats containing *Eogloecapsa* classified as "poor". Other coccoidal organisms, like *Entophysalis belcherensis* (2–5 μm in diameter) occur in dark patches and are never well-preserved (Figure 8). These mats are often classified as unrecognizable, and were assigned a percent area using Image J. Smaller coccoidal organisms, identified as *Sphaerophycus parvum* (2–3 μm), are abundant in many of the silicified microbial mats of the Angmaat Formation (Figure 8). However, the size of their cell is approximately the size of one to two pixels on the image mosaics, meaning that their morphological characteristics cannot be resolved; thus, these were discounted from the taphonomic counts. In many of the samples, clusters of these small, coccoidal microfossils were distributed throughout the preserved mat fabrics, and seemed to keep their spherical shape, but little could be determined regarding the ultrastructure of these organisms from light microscopy.

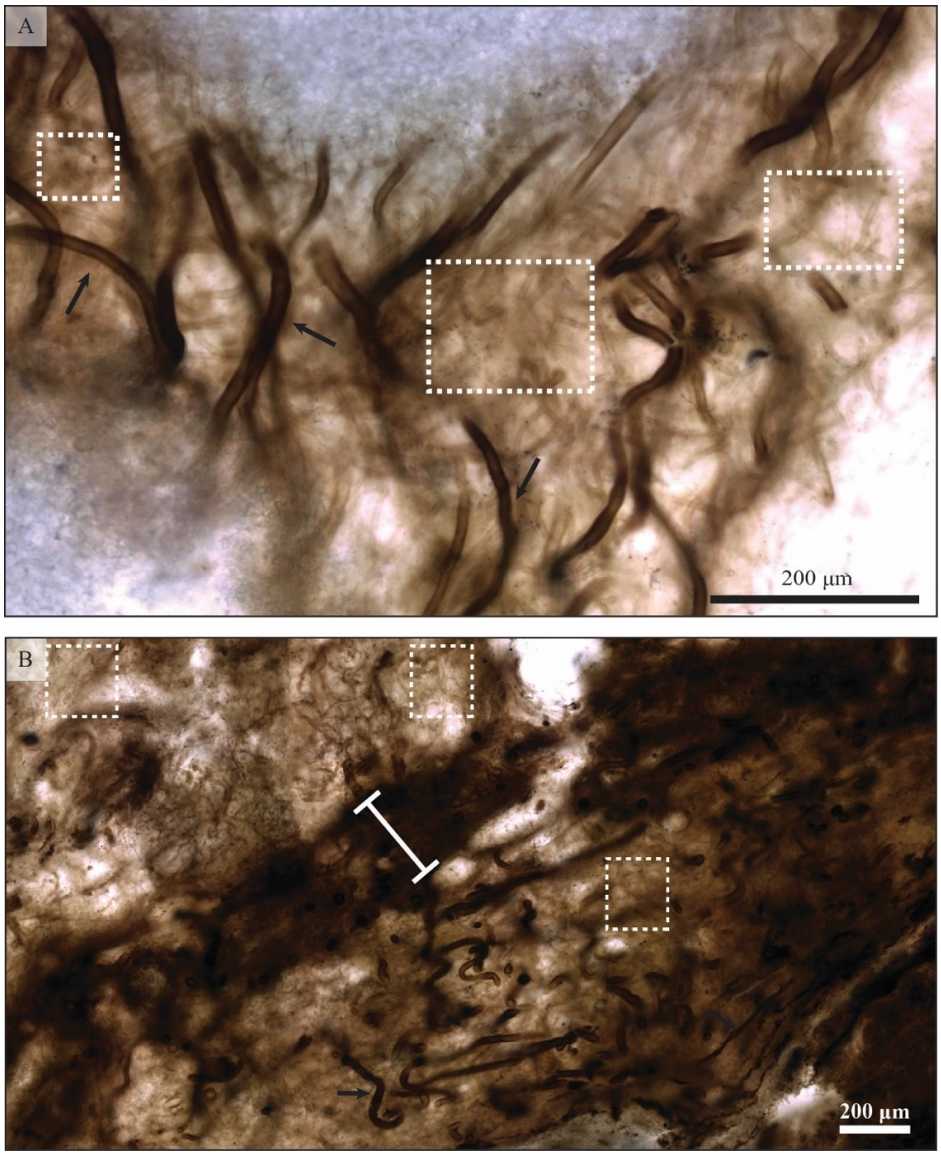

Figure 7. Primary components of filament-dominated mat fabrics. Two types of filamentous microfossils are observed in the Angmaat Formation mats. The large-diameter (25–40 micron), dark-colored filaments are sheaths of *Microcoleus* sp. and are highlighted with the black arrow in (**A**). Dark, compacted layers typically result from concentrations of *Microcoleus* sp. sheaths (**B**). White boxes highlight areas dominated by filamentous sheaths of *Siphonophycus* sp. (**A,B**). These thin-diameter (10–12 micron), light-colored filaments commonly lose their coloration during mat decomposition, which makes them difficult to assess during taphonomic analyses.

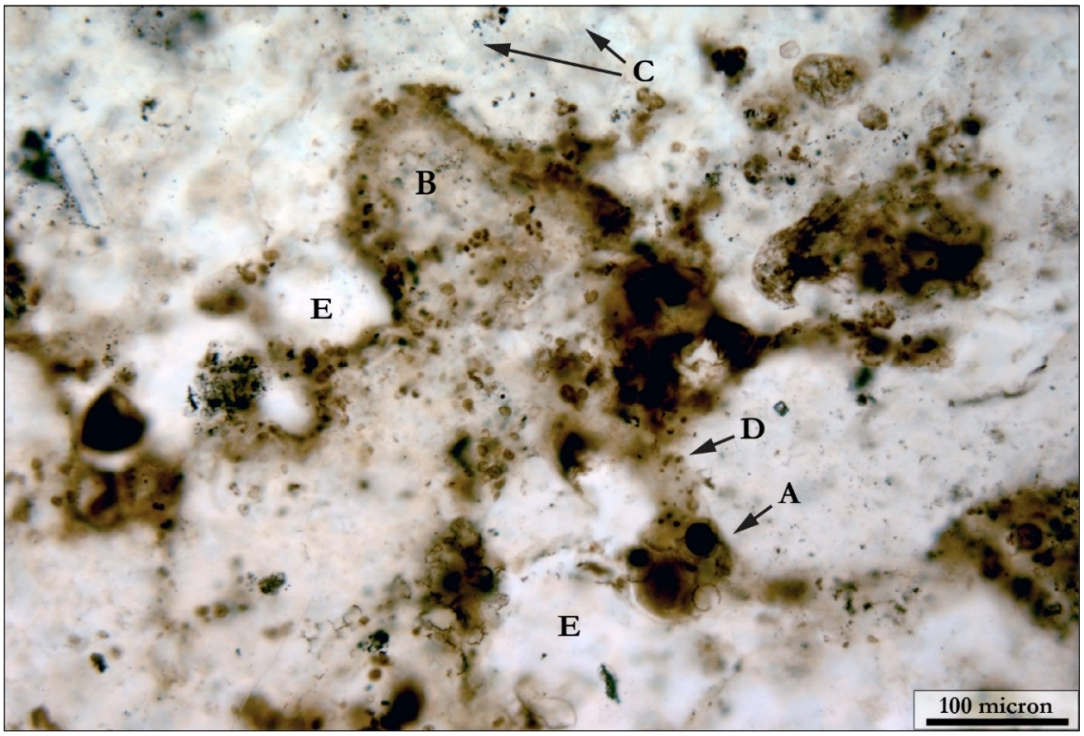

Figure 8. Complexity of mat fabrics. Coccoid-dominated mats commonly preserve a wide variety of coccoidal organisms, of different taphonomic state, within a matrix of silicified filament sheaths and extracellular polymeric substances (EPS). In this example, we see large individual coccoids (**A**), in clusters around a poorly preserved colony of *Eoentophysalis* sp. (**B**), embedded within a matrix consisting of very pale filament sheathes (**C**). Also, within this view, there are individual, micron-sized coccoids (**D**) embedded within regions of silicified EPS (**E**).

5.2. Results of Traditional Point-Counting

Traditional point-counting methods were performed with both light microscopy and image mosaics prior to development of the quadrat assessment methodology. Initially, results of traditional point-counting (i.e., via light microscopy) were compared to an assessment of the same sample performed on the mosaic, using the intersection of gridlines as a proxy for occular cross-hairs [58]. The results of this comparison are shown in Manning-Berg et al. [58]. The data indicate that although the point-counting methods are repeatable and can be translated to image mosaics, traditional point-counting methods are unable to address spatial variability within a preserved mat.

5.3. Results of Quadrat Sampling

Data from samples analyzed via the quadrat system are presented on ternary plots (Figures 10–18). The average composition was then compared to the preliminary, mesoscale visual assessment of the sample. Approximately 600 microfossils were classified for each of the seven samples that were classified as representing a range of mesoscale mat fabrics (Table 1). To ensure that the quadrat technique permitted an assessment of variability and was reproducible, analyses were first performed on a single sample, and then a second analysis was performed on the same sample several weeks later. Additionally, in order to determine the potential counts needed to accurately assess spatial variability within the mat, a complete assessment, that is, assessing a single quadrat in each of the 25 partitions, was performed a total of five times. If the random number generator selected a quadrat from within a partition that had been previously assessed, a new quadrat was selected by the random number generator. Each round was plotted on a ternary plot to assess the degree to which spatial heterogeneity affected taphonomic assessment of the entire thin section (Figure 10).

Table 1. Taphonomic assessment of the microfossils preserved in the Angmaat Formation. Individual microfossils were classified as "good", "fair", or "poor". Over 600 individual microfossils were counted using the quadrat method, and the percent area of unrecognizable carbonaceous matter was calculated with ImageJ over the entire thin section.

Sample	Classification	Organisms	Total Counts	Total Filament	Total Coccoid	% G	% F	% P	% Area Unrec
DBG-30	Good	Coccoidal	658	75	583	20	49	31	13.1
DBG-42	Fair	Coccoidal	659	283	376	1	28	71	6.1
DBN-4	Poor	Coccoidal	643	133	510	8	34	59	2.0
DAC-15	Good	Filamentous	609	553	56	11	35	53	0.5
DAC-24	Fair	Filamentous	149	148	1	1	41	58	3.6
DAC-16	Fair	Mixed	634	614	20	0	7	93	4.2
DAC-9	Poor	Mixed	175*	162	13	0	9	91	2.6

* Microfossils are rare in this sample, and only 175 microfossils were counted after two assays on the thin section.

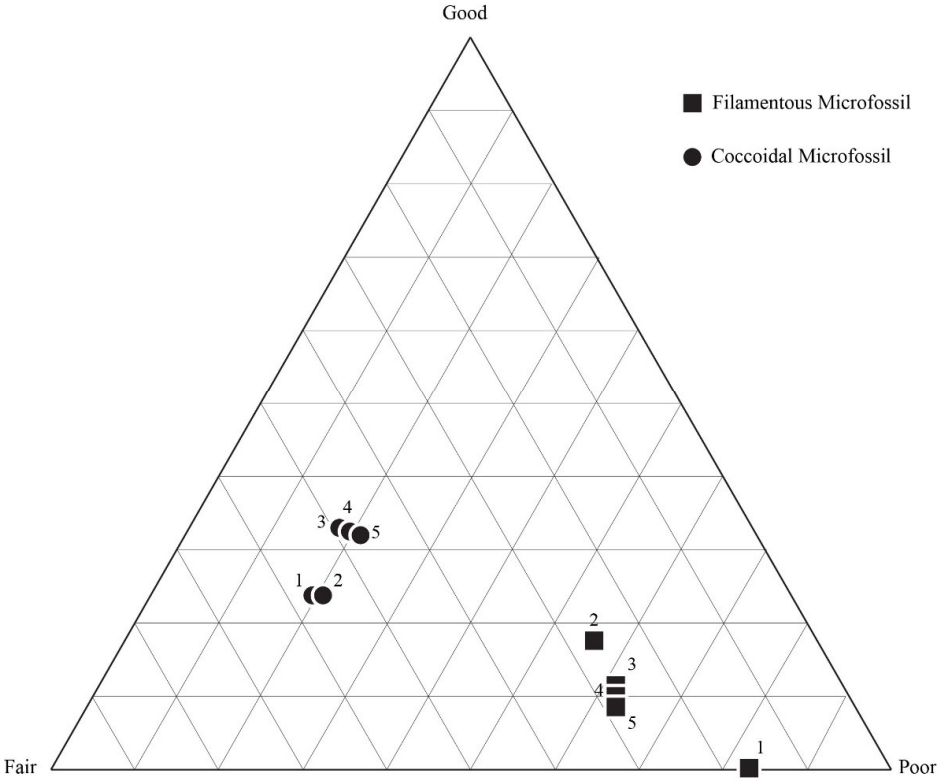

Figure 9. Taphonomic assessment of the sample (DAC-51). For this initial sample, fine individual taphonomic assessments were performed. Assessments were performed on different days to judge the consistency of the observer's taphonomic assessment. Additionally, different quadrats were assigned by a random number generator for each assessment to ascertain whether our quadrat sampling method was able to provide a representative assessment of the whole thin section.

The assessment of individual microfossils was collected in an Excel spreadsheet. Within this spreadsheet, data were presented as both the number of filaments and the total percentage of filaments, the number of coccoids and the total percentage of coccoids, and the percentages of the total microfossil count. Recording data in this way allowed for visualization of the complexity of the microbial mats at various scales. For example, Figure 10 shows data for a sample (DAC-15) that was visually identified on the mesoscopic scale as taphonomically "good" prior to the taphonomic assessment. To obtain 609 microfossil counts—here a total of 553 filaments and 56 coccoids—a total of 40 quadrats were included in the classification. Spatial variability in the taphonomy of the mat was readily noted by plotting individual quadrats on a ternary plot. In this sample, coccoids within one quadrat were assessed as taphonomically "good", coccoids in six quadrats were assessed as taphonomically "poor", and the other 37 quadrats preserved coccoidal morphologies that plotted within the "good–fair", "mixed", and "fair–poor" regions of the ternary plot [86]. Filament morphologies for this sample span the same

taphonomic range on the ternary plot, with the average filament classification plotting within the "fair–poor" region of the ternary plot. The coccoidal organisms in this sample had values that were influenced by more "good" preserved morphologies; thus, most plots were within the "mixed" portion of the ternary plot, as were the average coccoid data (Figure 12).

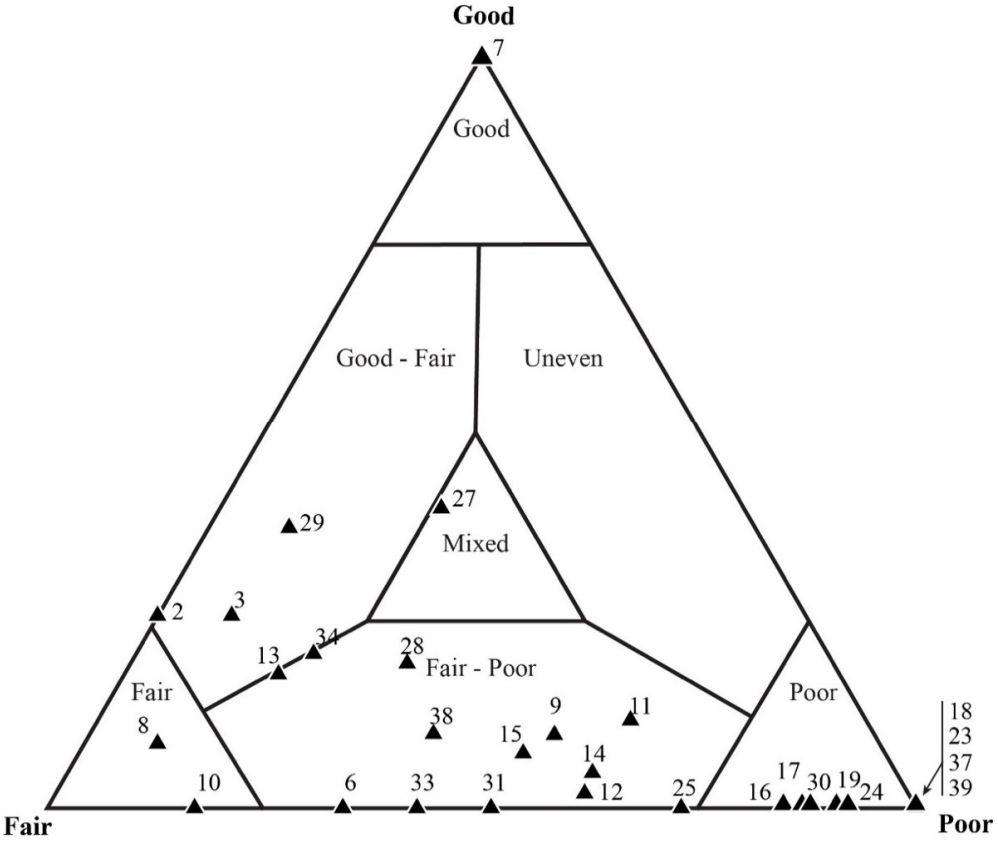

Figure 10. Taphonomic variation between quadrats in sample DAC-15. Each triangle represents the average taphonomic assessment of all microfossils (filaments and coccoids) within a single quadrat. To obtain the desired 600 microfossil count, 40 quadrats were counted. Each number corresponds to the quadrat number. Results show that a single sample can exhibit a wide range of preservation, resulting in individual quadrats plotting within several taphonomic fields. Such spatial variation would not be apparent with the averaging of all taphonomic data. Identification of such variation indicates that the quadrat method may be a powerful tool in the exploration of spatial variability within samples. Taphonomic fields were modeled after Kowalewski et al. (1995) [86].

Samples that were identified as taphonomically "fair" based on mesoscale visual inspection showed the greatest amount of variability when assessed via individual microfossil counts. Figure 12 shows the results of sample DBG-42, which only required that 25 quadrats be counted to obtain the desired 600 microfossils. A total of 659 microfossils were counted; 283 of these were represented by filamentous sheaths and 376 by coccoids. The microfossil counts, which included the number of filaments and coccoids in each quadrat, resulted in most data-plotting as being taphonomically "poor", with only 2 of the 25 quadrats plotting in the taphonomic range of "fair–poor". When focusing on the filamentous data alone, the data plot within the "poor" taphonomic range (Figure 13a). Coccoid-only data (Figure 13b) ranged from a "fair" to "fair–poor" preservation. The average taphonomy of all microfossils from DBG-42, however, plots within the "fair–poor" range. Similarly, a second sample, DAC-16, required counting 30 quadrats to obtain a count of 634 microfossils, including 614 filament sheaths and 20 coccoids. The total microfossil counts (number of filaments and coccoids) per each quadrat resulted in most data plotting as taphonomically "poor" (Figure 14). When looking at the

filamentous data alone (Figure 15a), all but one data plot is "poor". All but two of the quadrats, displaying the coccoid-only data for DAC-16, plot in the "fair" and "fair–poor" regions of the ternary plot (Figure 15b).

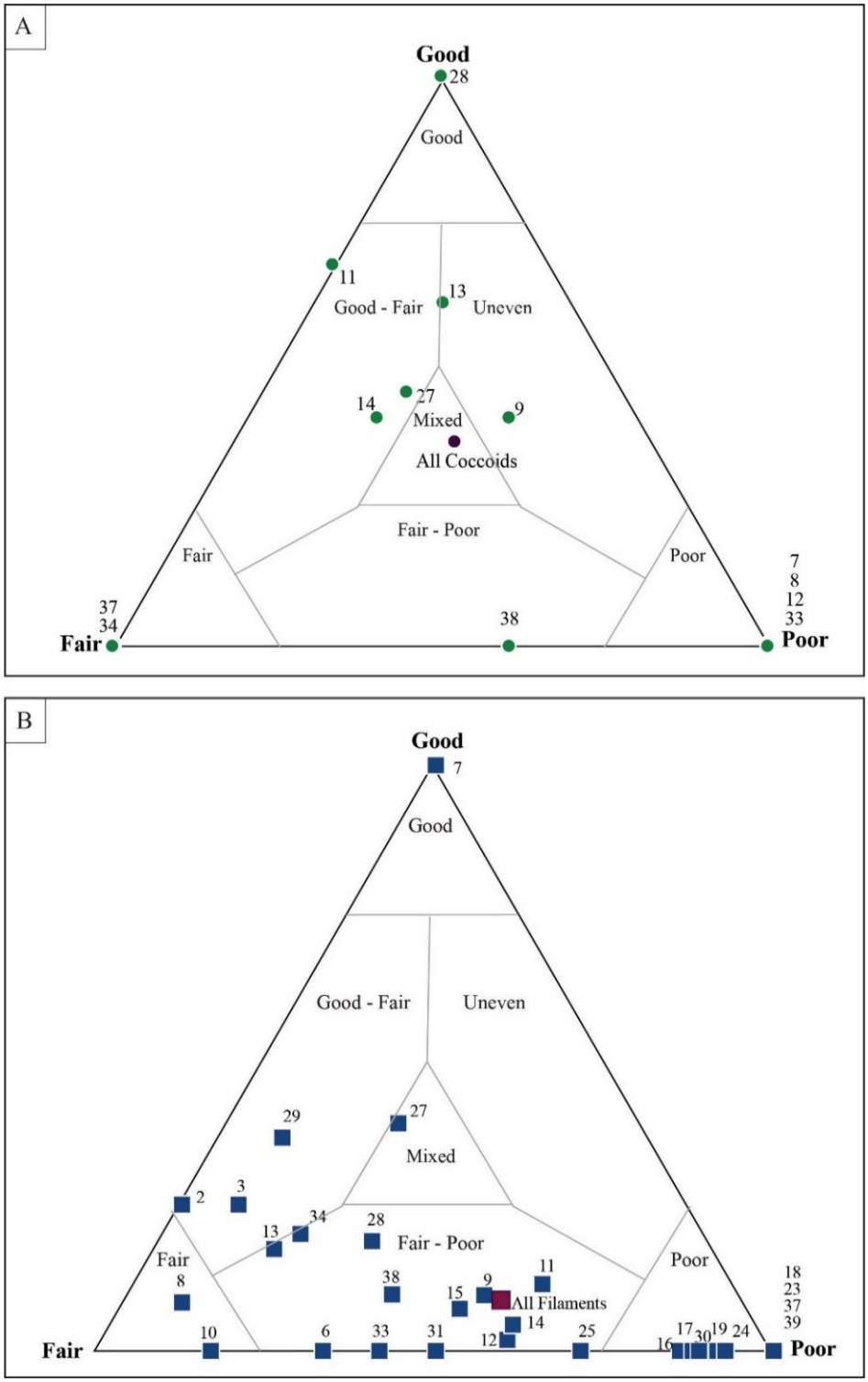

Figure 11. Assessment of coccoidal and filamentous microfossils in sample DAC-15. (**A**) Coccoidal microfossils show preservation range from "good" to "poor", but with an average taphonomic assessment of "mixed". (**B**) Filament sheaths are generally more abundant within the sample but are taphonomically more poorly preserved. Each data point represents a single, numbered quadrat.

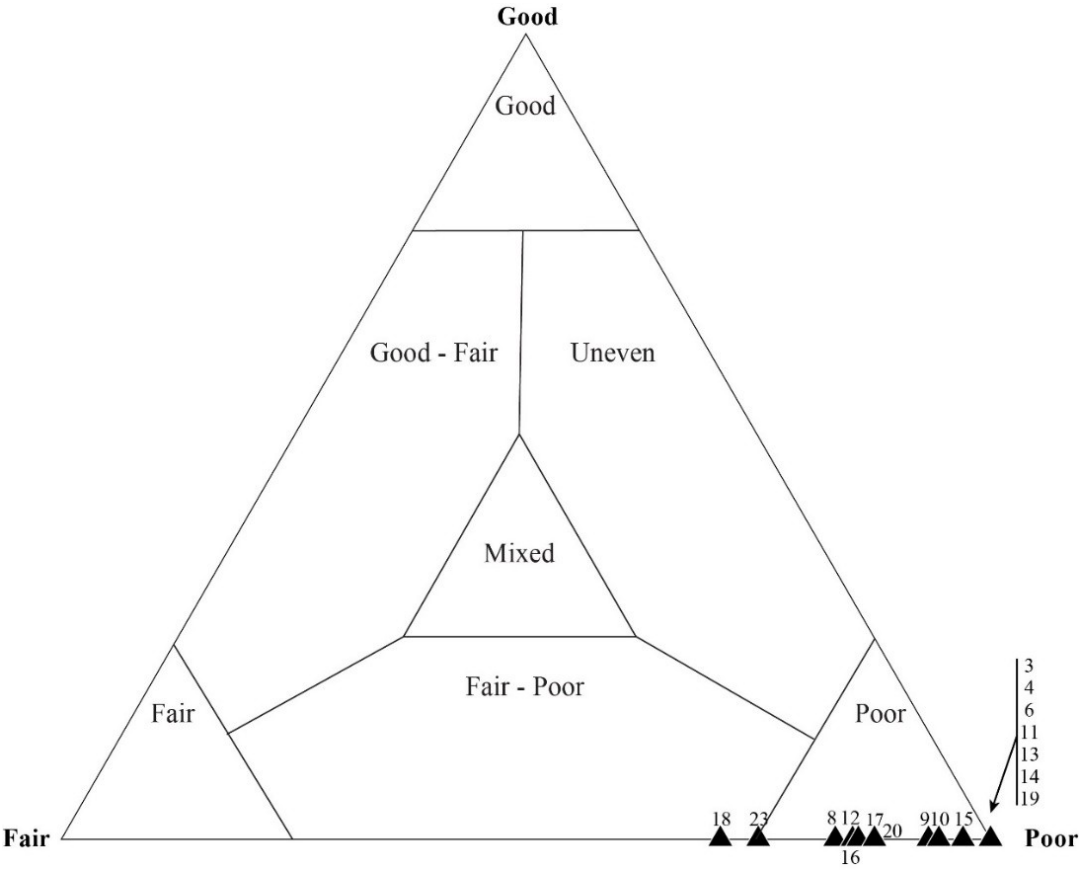

Figure 12. Taphonomic assessment of sample DBG-42. Even in a mat fabric that was originally assessed as "fair" in its preservation, most of the microfossils (coccoid and filament) occur within the taphonomic range of "poor".

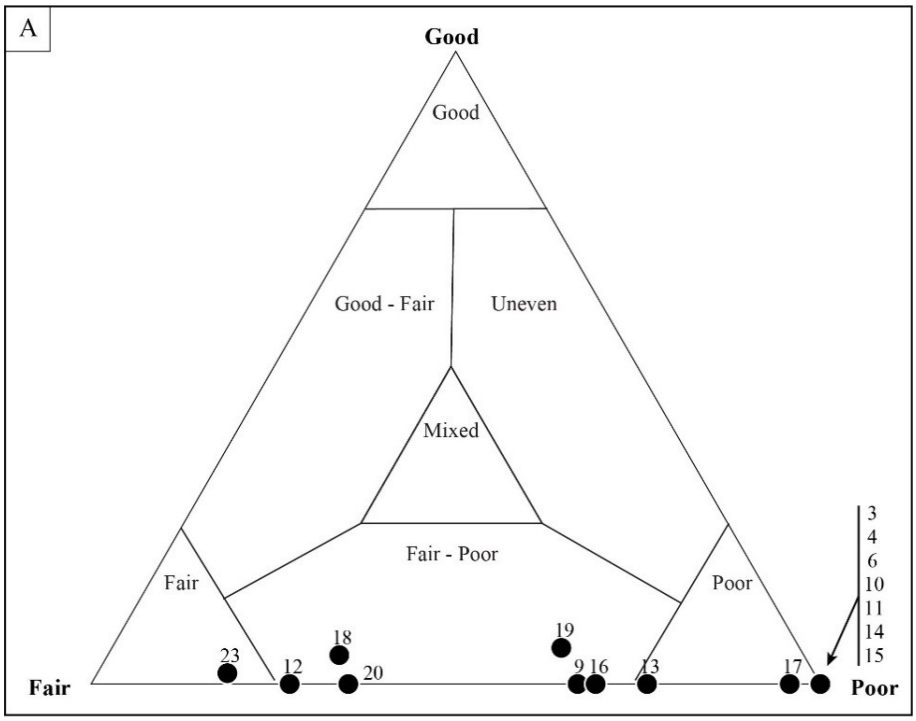

Figure 13. *Cont.*

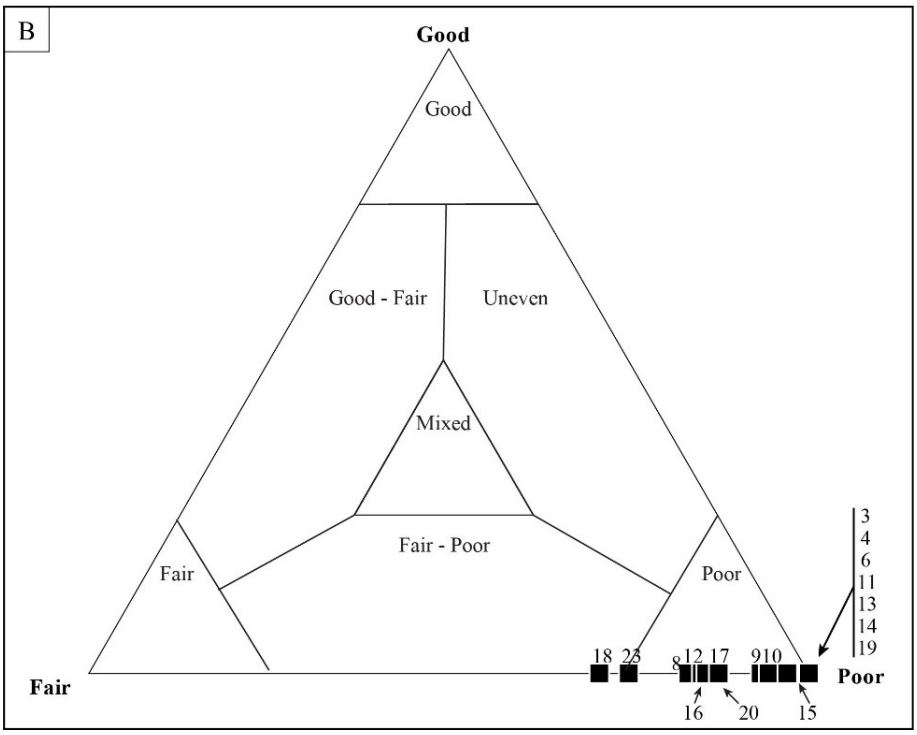

Figure 13. Quadrat data for DBG-42. As with Sample DAC-51, which was originally assessed as "good" (see Figure 12), (**A**) coccoidal microfossils generally show a wider range of taphonomic variability than (**B**) filamentous microfossils. Each data point represents a single, numbered quadrat.

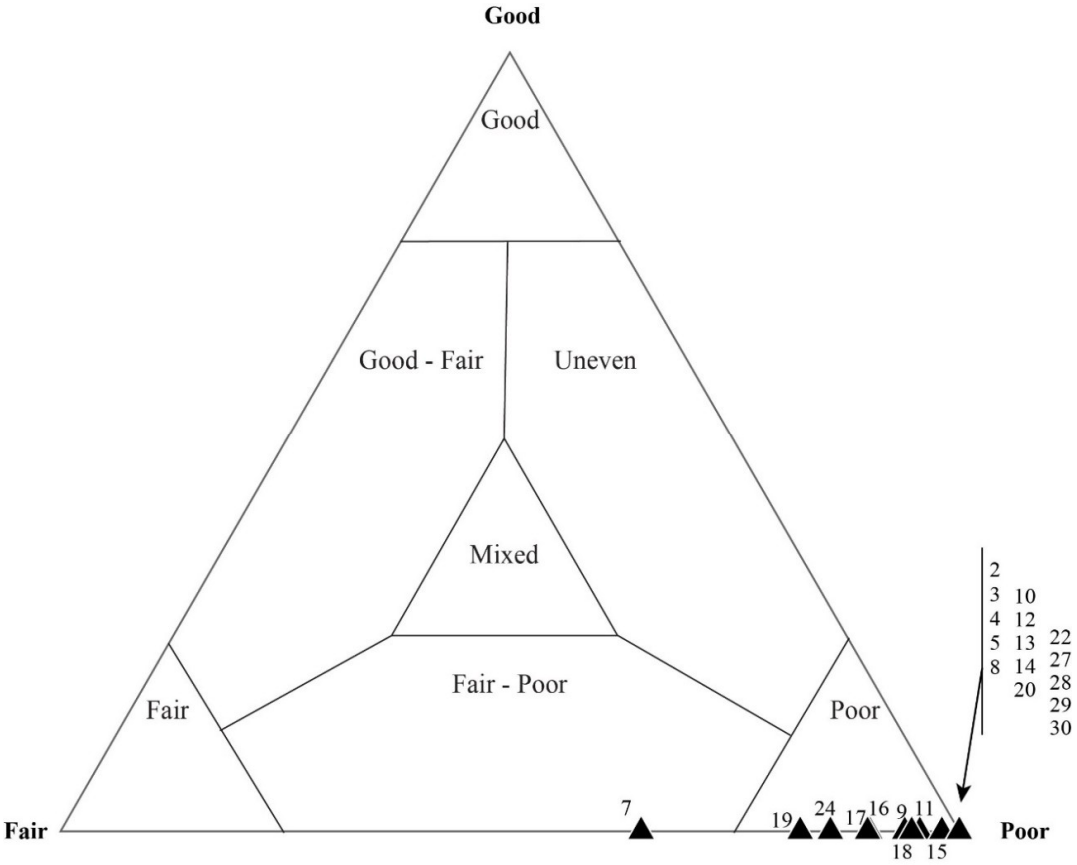

Figure 14. Taphonomic assessment of sample DAC-16. For a thin-section mat fabric originally classified as "poor", most of the microfossils (coccoid and filament) occur within the taphonomic range of "poor".

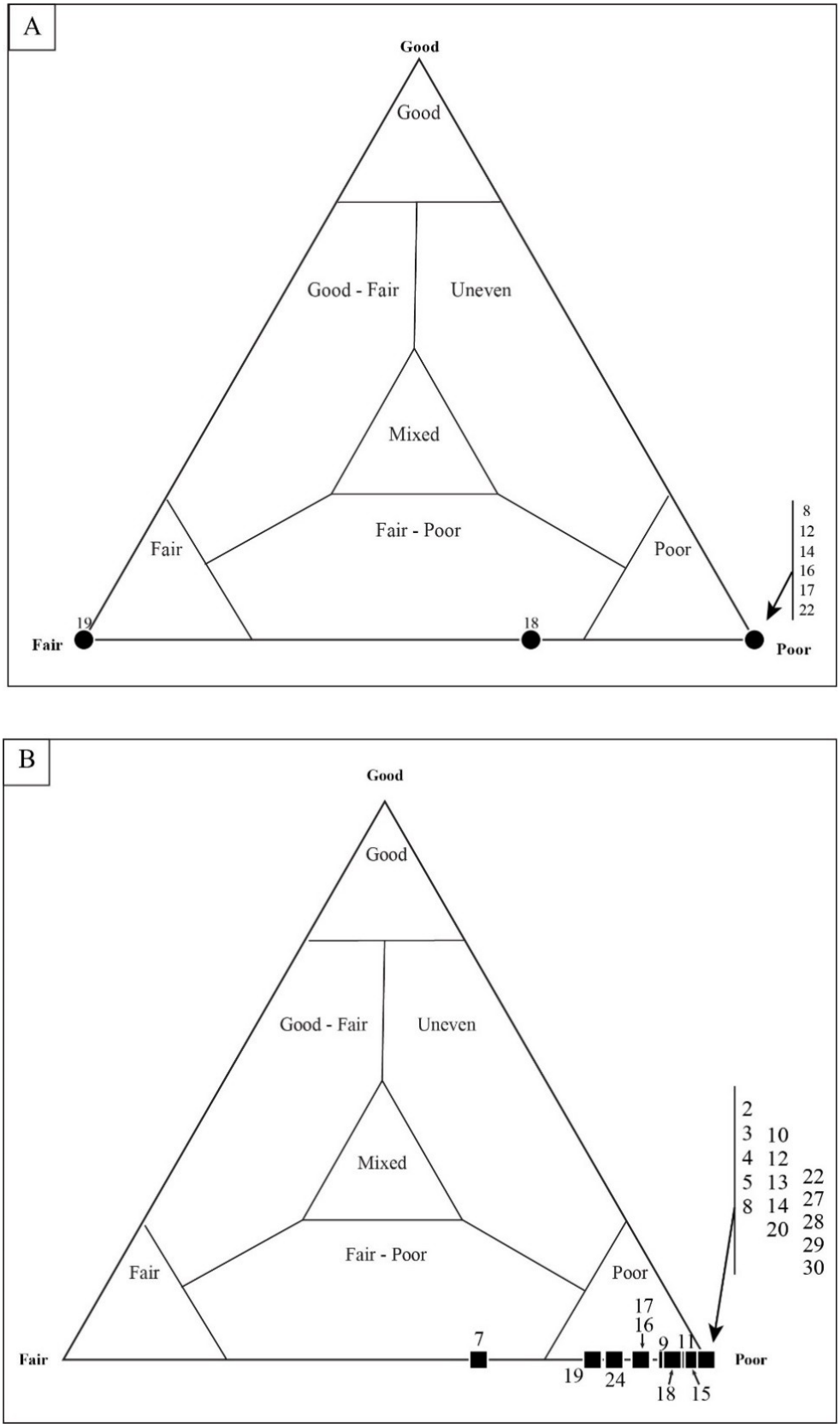

Figure 15. Quadrat data for DAC-16. As with other mat fabrics, (**A**) coccoidal microfossils show a wider range of taphonomic variation than (**B**) filamentous microfossils. Each data point represents a single, numbered quadrat.

A single sample, DBN-4, that was identified as taphonomically "poor" via mesoscale visual inspection, also showed variation at several scales. A total of 643 microfossils were counted from 25 quadrats. Of the microfossils, 113 were filaments and 510 were coccoids. Total microfossil assessments per quadrat (Figure 16) can be seen to vary between taphonomically "fair" to "poor". The filament classification plots along the "fair" to "poor" line of the ternary plot (Figure 17a). The coccoids, however, exhibit more variation, with some of the coccoidal microfossils plotting in the "good–fair", "mixed", and the "uneven" range (Figure 17b).

Altogether, the data indicate that the coccoids exhibit more variability in taphonomic range than the filamentous sheaths. Coccoidal fossils span taphonomic ranges from "good–fair", to "fair", to "poor". By contrast, filamentous sheaths plot in a narrower range of preservation, typically plotting within the "fair–poor" and "poor" regions. These trends are observed regardless of the taphonomic grade assigned to the mesoscale mat. In general, the mesoscale taphonomic grade corresponds well to the data collected on individual microfossils (Figure 18). Mat fabrics classified as "good" had a higher percentage of "good" individual microfossils for both coccoidal and filamentous mats. Variation between the quadrats within one sample plot across the entire taphonomic continuum in the ternary plot (Figure 11). The trend of data plotting as "good", through "good–fair" and "fair–poor" and ultimately to "poor", is the decomposition pattern observed in actualistic experiments [29].

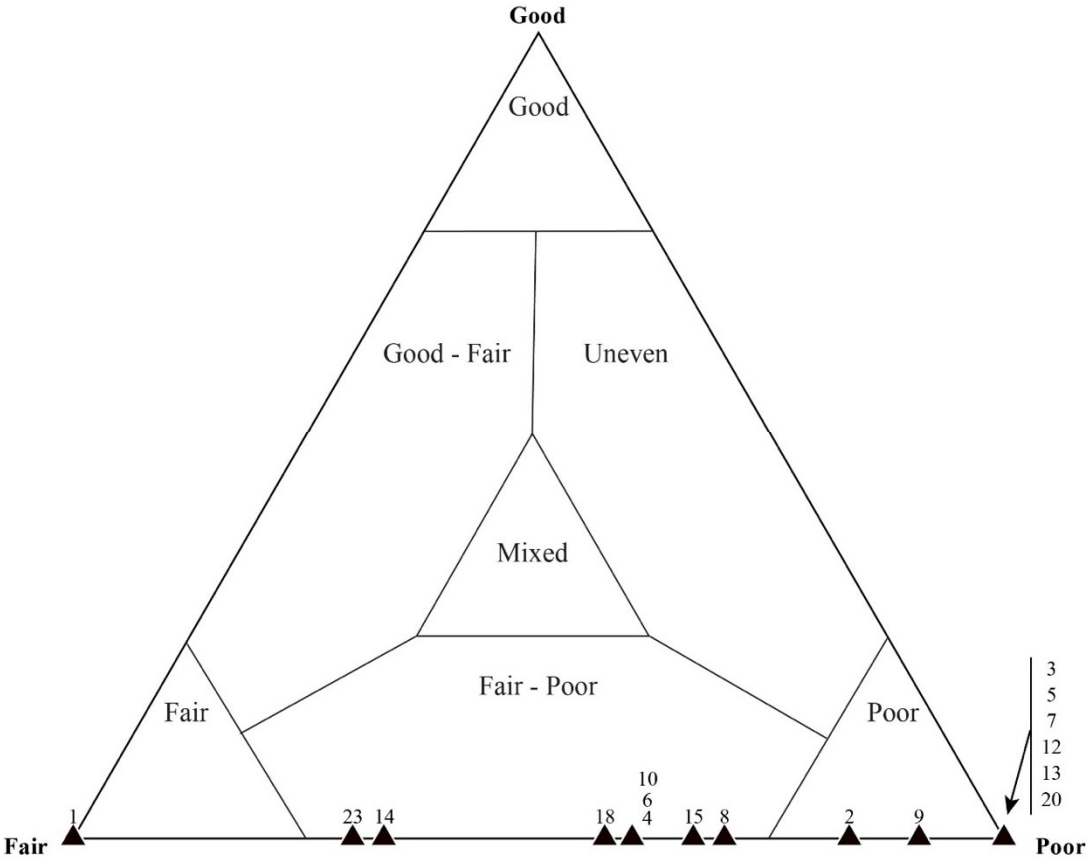

Figure 16. Taphonomic assessment of sample DBN-4. This thin section was originally assessed as a poorly preserved mat fabric. Most of the microfossils (coccoid and filament) occur within the taphonomic range of "fair–poor".

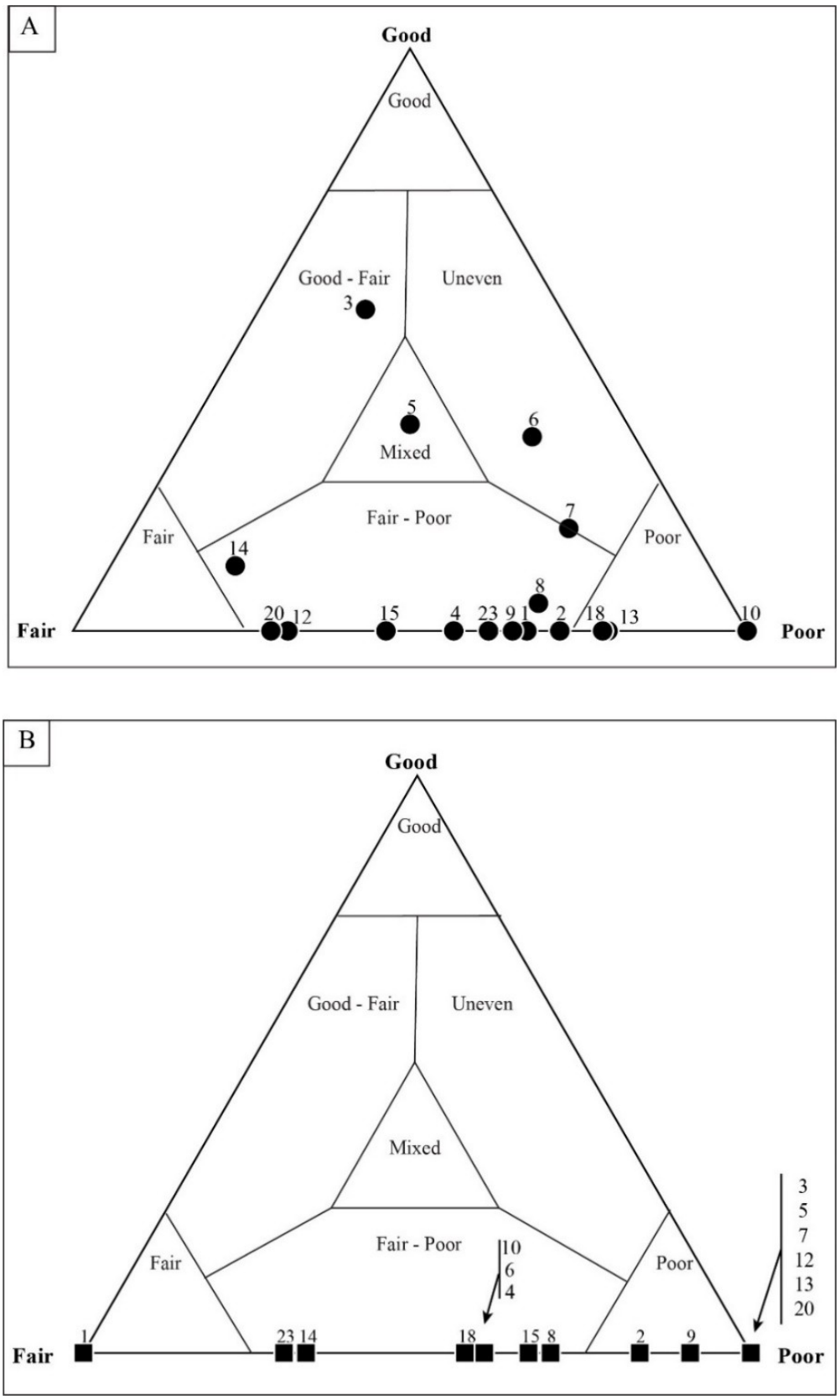

Figure 17. Quadrat data for DBN-4. Even within a generally poorly preserved mat fabric, (**A**) the taphonomy of coccoidal microfossils typically reflects better preservation than that of (**B**) filamentous microfossils. Each data point represents a single, numbered quadrat.

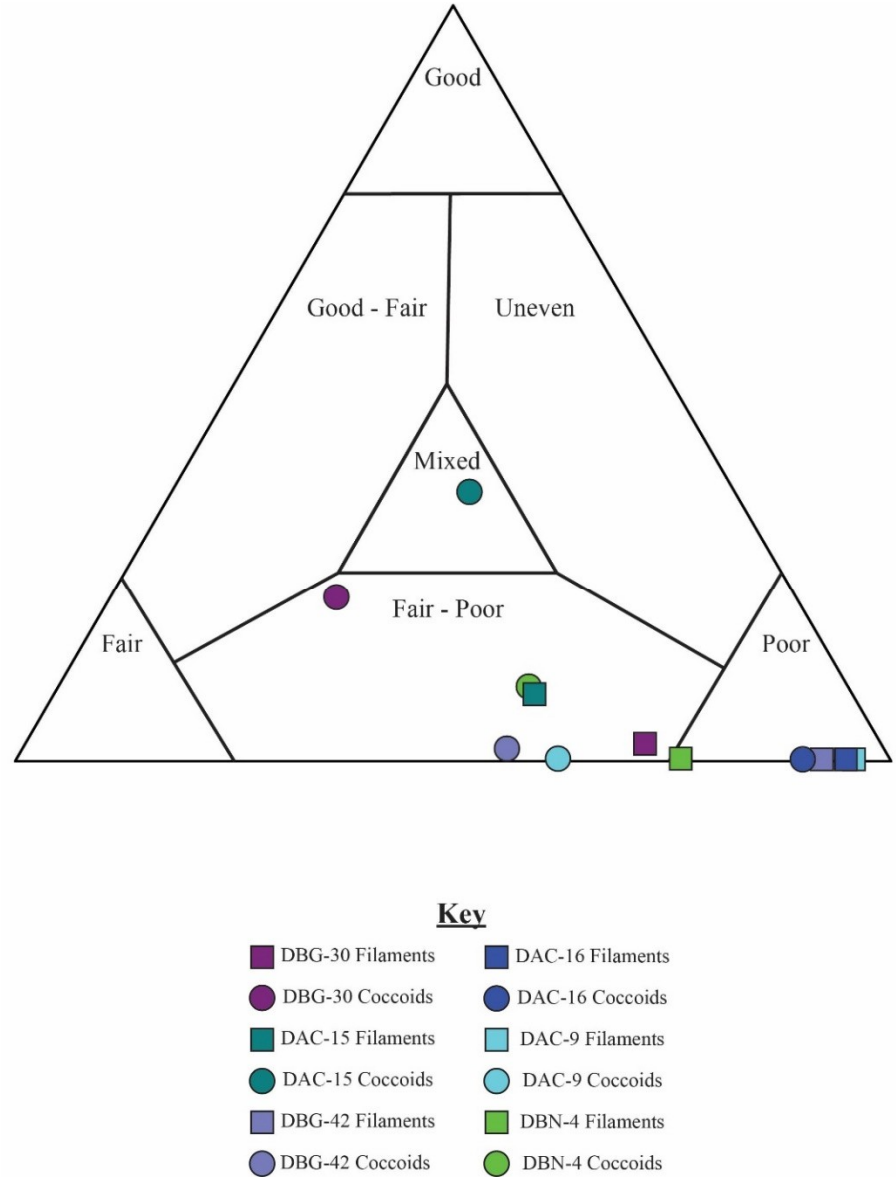

Figure 18. Quadrat data for six distinct samples. Circles represent data from coccoidal microfossil, which generally have a wider range of preserved taphonomic states. Squares represent data from filamentous microfossils, which plot consistently in the "poor" taphonomic range.

5.4. Raman Spectroscopy

Raman spectra were measured on ~144 microfossils from a total of 12 mat samples, which were visually determined to span the taphonomic grades of "good" to "unrecognizable". When possible, a "good", "fair", and "poor", example of the microfossils within one mat sample were chosen for analysis. In some cases, like in mat fabrics identified as "unrecognizable", the range of taphonomic preservation did not allow for "good", or even "fair" microfossils to be analyzed. Despite taphonomic variation in mat fabrics from the 12 samples and the individual microfossils analyzed, the shape and pattern of the Raman spectra were relatively similar (Figure 19). Spectra show peaks centered around 468 cm^{-1}, 1332 cm^{-1}, 1613 cm^{-1}, and 2938 cm^{-1}. The peak around 468 cm^{-1} is a quartz peak [95], which results from the chert matrix of the fossils. Peaks at 1332 cm^{-1} and 1613 cm^{-1} represent primary kerogen peaks, the D- and G-band, respectively [75]. As burial/diagenetic/metamorphic temperature increases, kerogen is thermally altered, which causes the shapes of the D- and G-bands to change as the D-band becomes sharper and narrower, losing a shoulder on the low wavenumber

end, and the G-band shifts to lower wavenumbers [76,96]. These changes are the result of increasing order within the macromolecular kerogen. Peaks centered around the D- and G-bands, however, show minor variation in the peak shape regardless of the taphonomic classification of the overall mat fabric within the Angmaat samples and the individual fossil being analyzed. The average Raman Index of Preservation (RIP) value [76] for the Angmaat Formation samples is 7.0 ± 0.4 (Table 2), where a value of 9 indicates that the preserved organic matter is immature and has not experienced much thermal alteration, and a value of 1 indicates that the organic matter has experienced substantial thermal alteration [97].

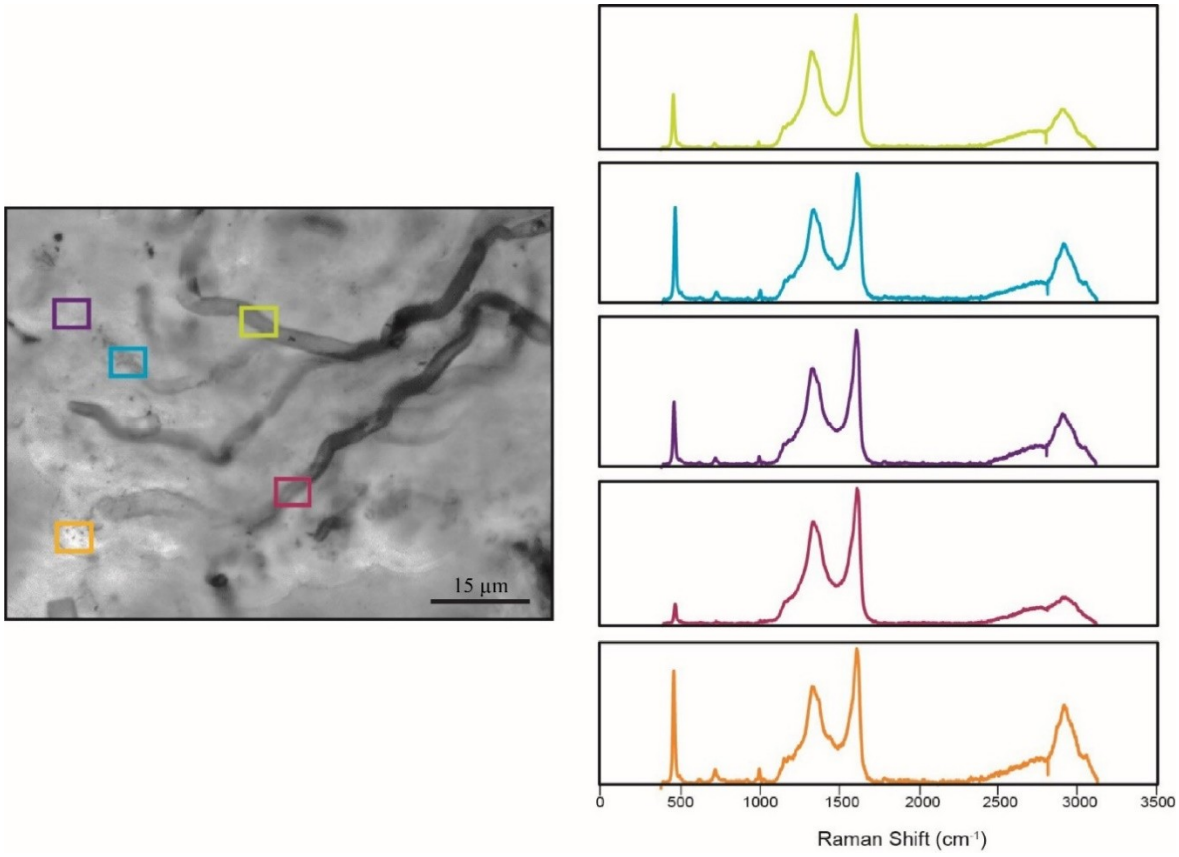

Figure 19. Raman analysis of individual microfossils. Filamentous microfossils can show preservation of distinctly different taphonomic states. Here, each box represents a location where the Raman point spectrum was collected. Despite the various taphonomic states of the microfossil, the Raman spectra obtained for each box have similar patterns, indicating that the taphonomic variation results from natural decomposition of the microfossils, and not from differential conditions of post-depositional diagenesis.

Table 2. Raman Index of Preservation values for the Angmaat Formation are around 7. Values closer to 1 are considered more highly altered samples, whereas values closer to 9 indicate less thermal alteration [57].

Sample	Taphonomic Classification	Average RIP	Average SD	*n*
DBG-30	Good	7.4	0.2	10
DAC-15	Good	6.6	0.3	13
DBG-42	Fair	7.3	0.3	13
DBN-4	Poor	7.0	0.3	13
DAC-18	Poor	6.6	0.2	17
Angmaat Average		7.0	0.4	66

6. Discussion

6.1. Taphonomic Analyses Using Quadrat Sampling on Image Mosaics

Performing a taphonomic assessment using image mosaics permits a more discrete exploration of complex mat fabrics. Specifically, the ability to move rapidly between various spatial scales allows a better understanding of the relationship between the overall mat fabric and the composition and taphonomic state of primary microbial constituents. Because the biological and geochemical gradients within a microbial mat should be reflected in both the composition and taphonomy of mat components, it is likely that preserved biochemical signatures may be fundamentally linked to mat taphonomy. Several studies have suggested the importance of taphonomic understanding in the interpretation of both early life on Earth and potential astrobiological signals [35,98–100]. Image mosaics and the taphonomic methods presented here can provide a detailed framework within which to explore the relationship between taphonomy and trends in isotopic, elemental, and molecular geochemistry.

High-resolution images also provide the opportunity to rapidly investigate thin sections at multiple scales, which provides a holistic view of microfossils and the relationship of an individual fossil to the overall mat morphology. The ability to partition large mosaics and to overlay grids for quadrat analysis greatly simplified taphonomic analysis and also provides multiple possibilities for displaying data, depending on the question being addressed. The system is also modular, making it easy to go back to a sample if the assessment of additional quadrats is necessary. Finally, image mosaics can be easily shared among research groups with different expertise and interests. In this study, the quadrat method was used to assess taphonomic variation over a thin section to compare the overall taphonomy of the preserved mat to geochemical analyses to be performed on bulk organic matter from the same samples. This method, however, is not limited to assessments of the whole sample, and could be a benefit for studies interested in determining the spatial resolution of microbial forms within a sample, or the diversity of elements within fossilized assemblages. This quadrat method could also be adapted for determining the cell density per unit area, or to further subdivide mat fabrics according to their taphonomic state.

The greatest difficulty with image mosaics is the size of the raw files, which easily overwhelm standard image processing software. For this reason, the images needed to be divided into partitions to be accessible using standard software. Other drawbacks include the fixed focal plane and limited depth of field for images within the mosaic. Taphonomic studies performed using light microscopy often utilize a variable focal plane to determine the three-dimensional character of a microfossil. With a fixed focal plane, it must be assumed that the portion of the microfossil that can be seen in the image is representative of the rest of the three-dimensional microfossil.

6.2. Mat Fabrics and Implications for Silicification

Microbial mats are complex ecosystems that grow by accretion. New mat growth occurs on top of the previous mat [7,10,101] and, internally, distinct microbial communities reflect geochemical gradients within the mat and preferred geochemical conditions of growth [7,10,102]. Together, these processes result in the preservation of characteristic laminated textures. As mats grow, the organic matter produced by photosynthesizing organisms is recycled by heterotrophic bacteria, which may inhibit the preservation of laminations [10,103]. However, in hypersaline mats where heterotrophic activity may be reduced, incomplete degradation of organic matter is commonly observed, which may ultimately preserve lamination [5,10]. This highlights the differences that microbial reworking of organic matter imparts on the taphonomic state of microbial mats, wherein incomplete degradation of organic matter would produce variation in both the condition of individual microfossils and overall mat fabrics. Therefore, taphonomy is a crucial component of Precambrian paleobiology studies and taphonomic processes largely affect the ultimate preservation state of a fossil or microbial mat in the fossil record [24,29,104–106]. In the case of Angmaat cherts, all samples, despite differences in mesoscale and microscale taphonomic state, contain individual microfossils that record thermally

immature organic matter. This indicates that taphonomic variation is best explained by the natural processes of microbial growth and degradation relative to the timing of silicification, and is not a reflection of post-depositional alteration of organic components.

Angmaat chert preserves a combination of filamentous and coccoidal microbial communities. Overall mat textures within the Angmaat Formation, however, appear to reflect taphonomic processes that acted differently, with respect to both the microbial constituents and the timing of silicification, and with respect to mat growth and decomposition. An average RIP value of 7 was obtained for each of the Angmaat chert samples. The consistency of the RIP values, both within individual samples and across the sample suite, indicates that the taphonomic variation of the microfossils is not the result of thermal alteration. Instead, taphonomic variation likely results entirely from the in situ biological degradation of mat components. Coccoidal organisms tend to record preservation across a wider range of taphonomic states, with more examples retaining markers of "good" preservation. During decomposition of coccoidal populations, cell walls readily shrink and form "spot cells" [107] within the cell that are often mistaken for an organelle or nucleus [80,85,107]. Within such populations, the presence or absence of cell shrinkage, which in experimental studies occurs over 10–125 days [29], provides a constraint on the timing of silicification relative to mat growth and decomposition. Similar loss of cellular material in coccoidal organisms is also observed in laboratory experiments involving the silicification of bacteria [94], commonly resulting in the homogenization of organic matter.

In the Angmaat chert samples, however, coccoid-dominated communities are commonly associated with substantial quantities of EPS. EPS, which consists of polysaccharides and exists as a gel, colloid, or in a dissolved state [108], protect organisms from rapid changes in the environment [108], such as the periodically exposed environments dominated by coccoidal communities [63]. We suggest that the presence of abundant EPS may play a critical role in the range of taphonomic states observed within coccoidal systems. First, the elevated water content of EPS may extend the ability of coccoidal communities to repair and retain their envelopes, even under conditions of exposure and desiccation [109]. Regions where EPS is abundant may be more resistant to compaction during mat decomposition. Finally, EPS is commonly associated with metal ions that are associated with mineral precipitation [110], and may enhance rates of polymerization during the process of early diagenetic silicification [41,111], which would also reduce the potential for decomposition of the coccoidal mat communities.

In this study, filamentous sheaths exhibited a narrower range in preservation and were most often classified as "poor". We suggest, however, that this observation reflects a fundamental bias that relates to the taphonomic pathway experienced by *Eomicrocoleus* sp. and *Siphonophycus* sp. communities. Sheaths of *Eomicrocoleus* sp. are large in diameter and are dark in color, which makes the microfossils readily identifiable in these mats. Sheaths of *Eomicrocoleus* sp., however, are relatively thin, flexible, and readily undergo compaction, resulting in a classification of "poor". By contrast, small-diameter sheaths of *Siphonophycus* sp. readily lose coloration. As a result, even though the robust, thick-walled sheaths of *Siphonophycus* sp. do not readily undergo compaction, they are not commonly able to be counted in a taphonomic assessment because they cannot be clearly identified.

Another interesting aspect of taphonomy in the filamentous communities is the rarity in which cellular trichomes are preserved. Filamentous cellular trichomes are commonly motile and can readily escape their sheaths. It is these empty, polysaccharide sheaths that are most commonly preserved in ancient samples [29,80,82,85,100]. Horodyski et al. [85] noted that even in modern microbial mats, less than 0.5% of sheaths preserved in the lower layers of the mats contained trichomes. In laboratory experiments involving the silicification of microorganisms, trichomes are also rarely preserved, and if they are preserved, the trichome is usually found outside of its sheath and severely deformed [81,94].

The motility of filamentous communities is most commonly inferred to reflect migration during diurnal cycles [6,11] in response to chemical gradients and changes in light quality and quantity [11], or with mat accretion, where trichomes naturally abandon their sheaths to form new ones at the mat surface [112]. Once the sheaths are empty, they are no longer maintained and are thus more

susceptible to taphonomic alteration [109,113]. The general absence of trichome preservation, combined with limited evidence for the structural decomposition of cyanobacterial sheaths, suggests that the process of silicification may play a role in the preservation of filamentous communities. Specifically, environmental stresses associated with the polymerization of silica during early diagenesis [64] may force trichomes to abandon their sheaths, thus favoring preservation of polysaccharide sheaths rather than cellular trichomes. Differences in the preservation of coccoidal and filamentous microfossils have been observed in other studies, but here we suggest that the difference in preservation is ecologically driven, reflecting the abandonment of sheaths by motile filaments.

Such exceptional preservation of microbial elements within Angmaat Formation permit a detailed investigation into microbial processes and, potentially, into the silicification process [64]. Because silicified microfossils comprise a substantial part of the preserved record of Proterozoic life [114], and are often considered ideal for preservation of Archean life [22], there is substantial impetus to understand how the range of taphonomy present in these samples [23,115] may reflect either the process of silicification, or the biogenicity of these more ancient samples. Further investigation of microbial assemblages that are convincingly biogenic will therefore provide critical insight into the preservation and biogenicity of more ancient samples.

7. Conclusions

The taphonomic assessment of silicified microbial mats within the Angmaat Formation, Baffin Island demonstrated the preserved complexity of microbial mats in the fossil record. Variation in preservation was observed at both the mesoscale (thin-section scale) and the microscale (individual microfossils) across the various taxa of organisms preserved, and between the morphologies of the individual microfossils. Mat fabrics were visually identified as "good", "fair", or "poor"; these classifications were then compared to the taphonomic assessment of individual microfossils within the mat. In general, the visual identification of the mesoscale mat fabric reflected the average composition of the individual microfossil morphologies. Coccoidal organisms consistently exhibited a wider range of preservation than their filamentous counterparts, which typically exhibited a narrow range of preservation in the "poor" taphonomic category. This observation may reflect differences in diagenetic pathways for filamentous organisms, which are motile and able to abandon their sheaths, and coccoidal organisms that are non-motile and insulated from changes in their environment by EPS.

Within this study, we described a new method for taphonomic assessment of microfossils using a quadrat template on image mosaics. Despite some issues regarding sample size and the limitations of a fixed focal plane, the image mosaics provided a more holistic view of the relationship of microfossils to overall mat morphologies. Image mosaics could also provide a template, or base map, for investigation of in situ geochemical preservation with taphonomic variation inherent to microbial mats. Such a use has far-reaching implications for improving our understanding of microfossil preservation in ancient samples, which is crucial for understanding early ecosystems and potential astrobiological targets.

Author Contributions: L.C.K. and A.R.M.-B. conceptualized this project, and A.R.M.-B. developed the pathway for project completion, including the taphonomic grading scheme, which reflected her earlier experiences with actualistic taphonomy. K.H.W. proposed the use of image mosaics for taphonomic assessment and aided in the creation of mosaics with equipment and software belonging to the Astrobiogeochemistry lab. The application of the quadrat sampling methodology for the image mosaics was developed by R.S.W. All of the Raman data was collected and analyzed with the help of instrumentation in Andrew Czaja's lab at the University of Cincinnati. The original draft of this manuscript was prepared by A.R.M.-B. as part of her Ph.D. dissertation. L.C.K., A.D.C., R.S.W. and K.H.W. reviewed and edited the manuscript. Samples from field seasons in 1993 and 1994 were provided by L.C.K. (field seasons funded by the National Geographic Society Committee for Research and Exploration).

Funding: Funding for this project was provided by a series of small grants to Ashley Manning-Berg from the Paleontological Society, the Society for Sedimentary Geology, The Society for Organic Petrology, and the Southeastern Section of the Geological Society of America. Image mosaics were completed at the Jet Propulsion Laboratory, California Institute of Technology, under a grant from the National Aeronautics and Space Administration.

Conflicts of Interest: The authors declare no conflict of interest. The funders had no role in the design of the study; in the collection, analyses, or interpretation of data; in the writing of the manuscript, or in the decision to publish the results.

References

1. van Gemerden, H. Marine Sediments, Burial, Pore Water Chemistry, Microbiology and Diagenesis Microbial mats: A joint venture. *Mar. Geol.* **1993**, *113*, 3–25. [CrossRef]
2. Sprachta, S.; Camoin, G.; Golubic, S.; Le Campion, T. Microbialites in a modern lagoonal environment: Nature and distribution, Tikehau atoll (French Polynesia). *Palaeogeogr. Palaeoclimatol. Palaeoecol.* **2001**, *175*, 103–124. [CrossRef]
3. Dupraz, C.; Reid, R.P.; Braissant, O.; Decho, A.W.; Norman, R.S.; Visscher, P.T. Processes of carbonate precipitation in modern microbial mats. *Earth-Sci. Rev.* **2009**, *96*, 141–162. [CrossRef]
4. Franks, J.; Stolz, J.F. Flat laminated microbial mat communities. *Earth-Sci. Rev.* **2009**, *96*, 163–172. [CrossRef]
5. Canfield, D.E.; Des Marais, D.J. Biogeochemical cycles of carbon, sulfur, and free oxygen in a microbial mat. *Geochim. Et Cosmochim. Acta* **1993**, *57*, 3971–3984. [CrossRef]
6. Dupraz, C.; Visscher, P.T. Microbial lithification in marine stromatolites and hypersaline mats. *Trends Microbiol.* **2005**, *13*, 429–438. [CrossRef] [PubMed]
7. Van Gemerden, H. Microbial mats: A joint venture. *Mar. Geol.* **1993**, *113*, 3–25. [CrossRef]
8. de Wit, R.; van den Ende, F.P.; van Gemerden, H. Mathematical simulation of the interactions among cyanobacteria, purple sulfur bacteria and chemotrophic sulfur bacteria in microbial mat communities. *Fems Microbiol. Ecol.* **1995**, *17*, 117–135. [CrossRef]
9. Herman, E.K.; Kump, L.R. Biogeochemistry of microbial mats under Precambrian environmental conditions: A modelling study. *Geobiology* **2005**, *3*, 77–92. [CrossRef]
10. Stal, L.J. Cyanobacterial Mats and Stromatolites. In *The Ecology of Cyanobacteria: Their Diversity in Time and Space*; Whitton, B.A., Potts, M., Eds.; Springer: Dordrecht, The Netherlands, 2002; pp. 61–120.
11. Stolz, J.F. Structure of Microbial Mats and Biofilms. In *Microbial Sediments*; Riding, R.E., Awramik, S.M., Eds.; Springer: Berlin/Heidelberg, Germany, 2000; pp. 1–8.
12. Wacey, D.; Kilburn, M.R.; Saunders, M.; Cliff, J.; Brasier, M.D. Microfossils of sulphur-metabolizing cells in 3.4-billion-year-old rocks of Western Australia. *Nat. Geosci.* **2011**, *4*, 698. [CrossRef]
13. Lepot, K.; Williford, K.H.; Ushikubo, T.; Sugitani, K.; Mimura, K.; Spicuzza, M.J.; Valley, J.W. Texture-specific isotopic compositions in 3.4 Gyr old organic matter support selective preservation in cell-like structures. *Geochim. Et Cosmochim. Acta* **2013**, *112*, 66–86. [CrossRef]
14. Sugitani, K.; Mimura, K.; Takeuchi, M.; Yamaguchi, T.; Suzuki, K.; Senda, R.; Asahara, Y.; Wallis, S.; Van Kranendonk, M.J. A Paleoarchean coastal hydrothermal field inhabited by diverse microbial communities: The Strelley Pool Formation, Pilbara Craton, Western Australia. *Geobiology* **2015**, *13*, 522–545. [CrossRef] [PubMed]
15. Brasier, M.; Green, O.; Lindsay, J.; Steele, A. Earth's Oldest (~3.5 Ga) Fossils and the 'Early Eden Hypothesis': Questioning the Evidence. *Orig. Life Evol. Biospheres* **2004**, *34*, 257–269. [CrossRef]
16. Schopf, J.W. Microfossils of the Early Archean Apex Chert: New Evidence of the Antiquity of Life. *Science* **1993**, *260*, 640–646. [CrossRef] [PubMed]
17. Wacey, D.; Saunders, M.; Kong, C.; Brasier, A.; Brasier, M. 3.46 Ga Apex chert 'microfossils' reinterpreted as mineral artefacts produced during phyllosilicate exfoliation. *Gondwana Res.* **2016**, *36*, 296–313. [CrossRef]
18. Brasier, M.D.; Green, O.R.; Lindsay, J.F.; McLoughlin, N.; Steele, A.; Stoakes, C. Critical testing of Earth's oldest putative fossil assemblage from the ~3.5 Ga Apex chert, Chinaman Creek, Western Australia. *Precambrian Res.* **2005**, *140*, 55–102. [CrossRef]
19. Schopf, J.W.; Kudryavtsev, A.B. Biogenicity of Earth's earliest fossils: A resolution of the controversy. *Gondwana Res.* **2012**, *22*, 761–771. [CrossRef]
20. Awramik, S.M.; Barghoorn, E.S. The Gunflint microbiota. *Precambrian Res.* **1977**, *5*, 121–142. [CrossRef]
21. Barghoorn, E.S.; Tyler, S.A. Microorganisms from the Gunflint Chert. *Science* **1965**, *147*, 563–577. [CrossRef]
22. Schopf, J.W. Microflora of the Bitter Springs Formation, Late Precambrian, Central Australia. *J. Paleontol.* **1968**, *42*, 651–688.

23. Wacey, D.; Menon, S.; Green, L.; Gerstmann, D.; Kong, C.; McLoughlin, N.; Saunders, M.; Brasier, M. Taphonomy of very ancient microfossils from the ~3400 Ma Strelley Pool Formation and ~1900 Ma Gunflint Formation: New insights using a focused ion beam. *Precambrian Res.* **2012**, *220–221*, 234–250. [CrossRef]
24. Knoll, A.H.; Strother, P.K.; Rossi, S. Distribution and diagenesis of microfossils from the lower proterozoic duck creek dolomite, Western Australia. *Precambrian Res.* **1988**, *38*, 257–279. [CrossRef]
25. Knoll, A.H.; Swett, K.; Mark, J. Paleobiology of a Neoproterozoic Tidal Flat/Lagoonal Complex: The Draken Conglomerate Formation, Spitsbergen. *J. Paleontol.* **1991**, *65*, 531–570. [CrossRef] [PubMed]
26. Sergeev, V.N.; Knoll, A.H.; Grotzinger, J.P. Paleobiology of the Mesoproterozoic Billyakh Group, Anabar Uplift, Northern Siberia. *J. Paleontol.* **1995**, *39*, 1–37.
27. Horodyski, R.J.; Donaldson, J.A. Microfossils from the Middle Proterozoic Dismal Lakes Groups, Arctic Canada. *Precambrian Res.* **1980**, *11*, 125–159. [CrossRef]
28. Horodyski, R.J.; Donaldson, J.A. Distribution and Significance of Microfossils in Cherts of the Middle Proterozoic Dismal Lakes Group, District of Mackenzie, Northwest Territories, Canada. *J. Paleontol.* **1983**, *57*, 271–288.
29. Bartley, J.K. Actualistic Taphonomy of Cyanobacteria: Implications for the Precambrian Fossil Record. *PALAIOS* **1996**, *11*, 571–586. [CrossRef]
30. French, K.L.; Hallmann, C.; Hope, J.M.; Schoon, P.L.; Zumberge, J.A.; Hoshino, Y.; Peters, C.A.; George, S.C.; Love, G.D.; Brocks, J.J.; et al. Reappraisal of hydrocarbon biomarkers in Archean rocks. *Proc. Natl. Acad. Sci. USA* **2015**, *112*, 5915–5920. [CrossRef]
31. DeGregorio, B.T.; Sharp, T.G.; Flynn, G.; Wirick, S.; Hervig, R.L. Biogenic origin for Earth's oldest putative microfossils. *Geology* **2009**, *37*, 631–634. [CrossRef]
32. Qu, Y.; Engdahl, A.; Zhu, S.; Vajda, V.; McLoughlin, N. Ultrastructural Heterogeneity of Carbonaceous Material in Ancient Cherts: Investigating Biosignature Origin and Preservation. *Astrobiology* **2015**, *15*, 825–842. [CrossRef]
33. Igisu, M.; Ueno, Y.; Shimojima, M.; Nakashima, S.; Awramik, S.M.; Ohta, H.; Maruyama, S. Micro-FTIR spectroscopic signatures of Bacterial lipids in Proterozoic microfossils. *Precambrian Res.* **2009**, *173*, 19–26. [CrossRef]
34. Hickman-Lewis, K.; Garwood, R.J.; Withers, P.J.; Wacey, D. X-ray microtomography as a tool for investigating the petrological context of Precambrian cellular remains. *Geol. Soc. Lond. Spec. Publ.* **2017**, *448*, 33–56. [CrossRef]
35. Guo, Z.; Peng, X.; Czaja, A.D.; Chen, S.; Ta, K. Cellular taphonomy of well-preserved Gaoyuzhuang microfossils: A window into the preservation of ancient cyanobacteria. *Precambrian Res.* **2018**, *304*, 88–98. [CrossRef]
36. Lemelle, L.; Labrot, P.; Salomé, M.; Simionovici, A.; Viso, M.; Westall, F. In situ imaging of organic sulfur in 700–800 My-old Neoproterozoic microfossils using X-ray spectromicroscopy at the S K-edge. *Org. Geochem.* **2008**, *39*, 188–202. [CrossRef]
37. Oehler, D.Z.; Robert, F.; Walter, M.R.; Sugitani, K.; Allwood, A.; Meibom, A.; Mostefaoui, S.; Selo, M.; Thomen, A.; Gibson, E.K. NanoSIMS: Insights to biogenicity and syngeneity of Archaean carbonaceous structures. *Precambrian Res.* **2009**, *173*, 70–78. [CrossRef]
38. Thomen, A.; Robert, F.; Remusat, L. Determination of the nitrogen abundance in organic materials by NanoSIMS quantitative imaging. *J. Anal. At. Spectrom.* **2014**, *29*, 512–519. [CrossRef]
39. Benzerara, K.; Menguy, N. Looking for traces of life in minerals. *Comptes Rendus Palevol* **2009**, *8*, 617–628. [CrossRef]
40. Hesse, R. Silica diagenesis: Origin of inorganic and replacement cherts. *Earth-Sci. Rev.* **1989**, *26*, 253–284. [CrossRef]
41. Iler, R.K. *Chemistry of Silica—Solubility, Polymerization, Colloid and Surface Properties and Biochemistry*; John Wiley & Sons: Hoboken, NJ, USA, 1979.
42. Mizutani, S. Silica Minerals in the Early Stage of Diagenesis. *Sedimentology* **1970**, *15*, 419–436. [CrossRef]
43. Siever, R. Silica Solubility, 0–200 °C, and the Diagenesis of Siliceous Sediments. *J. Geol.* **1962**, *70*, 127–150. [CrossRef]
44. Williams, L.A.; Crerar, D.A. Silica diagenesis; II, General mechanisms. *J. Sediment. Res.* **1985**, *55*, 312–321. [CrossRef]

45. Williams, L.A.; Parks, G.A.; Crerar, D.A. Silica diagenesis; I, Solubility controls. *J. Sediment. Res.* **1985**, *55*, 301–311. [CrossRef]
46. Alleon, J.; Bernard, S.; Le Guillou, C.; Daval, D.; Skouri-Panet, F.; Pont, S.; Delbes, L.; Robert, F. Early entombment within silica minimizes the molecular degradation of microorganisms during advanced diagenesis. *Chem. Geol.* **2016**, *437*, 98–108. [CrossRef]
47. Oehler, J.H.; Schopf, J.W. Artificial Microfossils: Experimental Studies of Permineralization of Blue-Green Algae in Silica. *Science* **1971**, *174*, 1229–1231. [CrossRef]
48. Orange, F.; Lalonde, S.V.; Konhauser, K.O. The Formation and Preservation of Synechococcus elongatus Cell Molds in Simulated Silica Sinter: Implications for the Identification of Microfossils. *Geomicrobiol. J.* **2013**, *30*, 327–336. [CrossRef]
49. Phoenix, V.R.; Adams, D.G.; Konhauser, K.O. Cyanobacterial viability during hydrothermal biomineralisation. *Chem. Geol.* **2000**, *169*, 329–338. [CrossRef]
50. Yee, N.; Phoenix, V.R.; Konhauser, K.O.; Benning, L.G.; Ferris, F.G. The effect of cyanobacteria on silica precipitation at neutral pH: Implications for bacterial silicification in geothermal hot springs. *Chem. Geol.* **2003**, *199*, 83–90. [CrossRef]
51. Igisu, M.; Yokoyama, T.; Ueno, Y.; Nakashima, S.; Shimojima, M.; Ohta, H.; Maruyama, S. Changes of aliphatic C–H bonds in cyanobacteria during experimental thermal maturation in the presence or absence of silica as evaluated by FTIR microspectroscopy. *Geobiology* **2018**, *16*, 412–428. [CrossRef]
52. Benning, L.G.; Phoenix, V.R.; Yee, N.; Konhauser, K.O. The dynamics of cyanobacterial silicification: An infrared micro-spectroscopic investigation1. *Geochim. Et Cosmochim. Acta* **2004**, *68*, 743–757. [CrossRef]
53. Dunham, J.I.; Kah, L.C. Understanding 'gridwork' textures within Proterozoic early diagenetic chert. In Proceedings of the Geological Society of America Annual Meeting, Seattle, WA, USA, 22–25 October 2017.
54. Jackson, G.; Iannelli, T. Rift-related cyclic sedimentation in the Neohelikian Borden Basin, northern Baffin Island. *Geol. Surv. Can. Pap.* **1981**, *81*, 269–302.
55. Kah, L.C.; Knoll, A.H. Microbenthic distribution of Proterozoic tidal flats: Environmental and taphonomic considerations. *Geology* **1996**, *24*, 79–82. [CrossRef]
56. Kah, L.C.; Sherman, A.G.; Narbonne, G.M.; Knoll, A.H.; Kaufman, A.J. δ13C stratigraphy of the Proterozoic Bylot Supergroup, Baffin Island, Canada: Implications for regional lithostratigraphic correlations. *Can. J. Earth Sci.* **1999**, *36*, 313–332. [CrossRef]
57. Turner, E.C. Mesoproterozoic carbonate systems in the Borden Basin, Nunavut. *Can. J. Earth Sci.* **2009**, *46*, 915–938. [CrossRef]
58. Manning-Berg, A.R.; Kah, L.C.; Williford, K.H. Evaluation of preliminary techniques used to assess taphonomic variation in silicified microbial mats preserved in the Angmaat Formation, northern Baffin Island, Nunavut. In *Summary of Activities 2018 Canada-Nunavut Geoscience Office*; Canada-Nunavut Geoscience Office: Iqaluit, NU, Canada, 2018.
59. Hahn, K.E.; Turner, E.C.; Babechuk, M.G.; Kamber, B.S. Deep-water seep-related carbonate mounds in a Mesoproterozoic alkaline lake, Borden Basin (Nunavut, Canada). *Precambrian Res.* **2015**, *271*, 173–197. [CrossRef]
60. Sherman, A.G.; James, N.P.; Narbonne, G.M. Evidence for reversal of basin polarity during carbonate ramp development in the Mesoproterozoic Borden Basin, Baffin Island. *Can. J. Earth Sci.* **2002**, *39*, 519–538. [CrossRef]
61. Kah, L.C. Sedimentological, Geochemical, and Paleobiological Interactions on a Mesoproterozoic Carbonate Platform: Society Cliffs Formation, Northern Baffin Island, Arctic Canada. Ph.D. Thesis, Harvard University, Cambridge, MA, USA, 1997.
62. Kah, L.C.; Bartley, J.K. Protracted oxygenation of the Proterozoic biosphere. *Int. Geol. Rev.* **2011**, *53*, 1424–1442. [CrossRef]
63. Knoll, A.H.; Wörndle, S.; Kah, L.C. Covariance of microfossil assemblages and microbialite textures across an upper Mesoproterozoic carbonate platform. *Palaios* **2013**, *28*, 453–470. [CrossRef]
64. Manning-Berg, A.R.; Kah, L.C. Proterozoic microbial mats and their constraints on environments of silicification. *Geobiology* **2017**, *15*, 469–483. [CrossRef] [PubMed]
65. Turner, E.C. Structural and Stratigraphic Controls on Carbonate-Hosted Base Metal Mineralization in the Mesoproterozoic Borden Basin (Nanisivik District), Nunavut. *Econ. Geol.* **2011**, *106*, 1197–1223. [CrossRef]

66. Sherman, A.G.; Narbonne, G.M.; James, N.P. Anatomy of a cyclically packaged Mesoproterozoic carbonate ramp in northern Canada. *Sediment. Geol.* **2001**, *139*, 171–203. [CrossRef]
67. Narbonne, G.M.; James, N.P. Mesoproterozoic deep-water reefs from Borden Peninsula, Arctic Canada. *Sedimentology* **1996**, *43*, 827–848. [CrossRef]
68. LeCheminant, A.N.; Heaman, L.M. Mackenzie igneous events, Canada: Middle Proterozoic hotspot magmatism associated with ocean opening. *Earth Planet. Sci. Lett.* **1989**, *96*, 38–48. [CrossRef]
69. Gibson, T.M.; Shih, P.M.; Cumming, V.M.; Fischer, W.W.; Crockford, P.W.; Hodgskiss, M.S.W.; Wörndle, S.; Creaser, R.A.; Rainbird, R.H.; Skulski, T.M.; et al. Precise age of Bangiomorpha pubescens dates the origin of eukaryotic photosynthesis. *Geology* **2018**, *46*, 135–138. [CrossRef]
70. Kah, L.C.; Bartley, J.K.; Teal, D.A. Chemostratigraphy of the Late Mesoproterozoic Atar Group, Taoudeni Basin, Mauritania: Muted isotopic variability, facies correlation, and global isotopic trends. *Precambrian Res.* **2012**, *200–203*, 82–103. [CrossRef]
71. Pehrsson, S.J.; Buchan, K.L. Borden dykes of Baffin Island, Northwest Territories: A Franklin U-Pb baddeleyite age and a paleomagnetic reinterpretation. *Can. J. Earth Sci.* **1999**, *36*, 65–73. [CrossRef]
72. Hofmann, H.J.; Jackson, G.D. Shelf-Facies Microfossils from the Uluksan Group (Proterozoic Bylot Supergroup), Baffin Island, Canada. *J. Paleontol.* **1991**, *65*, 361–382. [CrossRef]
73. Golovenok, V.; Belova, M.Y. Rifeyskiye mikrobioty v kremnyakh iz billyakhskoy serii Anabarskogo podniatiya [Riphean microbiotas in cherts of the Billyakh Group on the Anabar Uplift]. *Paleontologicheskii Zhurnal* **1984**, *4*, 23–32.
74. Green, J.W.; Knoll, A.H.; Golubi, X.S.; Swett, K. Paleobiology of Distinctive Benthic Microfossils from the Upper Proterozoic Limestone-Dolomite "Series," Central East Greenland. *Am. J. Bot.* **1987**, *74*, 928–940. [CrossRef]
75. Butterfield, N.J. Bangiomorpha pubescens n. gen., n. sp.: Implications for the evolution of sex, multicellularity, and the Mesoproterozoic/Neoproterozoic radiation of eukaryotes. *Paleobiology* **2000**, *26*, 386–404. [CrossRef]
76. Schopf, J.W.; Kudryavtsev, A.B.; Agresti, D.G.; Czaja, A.D.; Wdowiak, T.J. Raman imagery: A new approach to assess the geochemical maturity and biogenicity of permineralized Precambrian fossils. *Astrobiology* **2005**, *5*, 333–371. [CrossRef]
77. Czaja, A.D.; Beukes, N.J.; Osterhout, J.T. Sulfur-oxidizing bacteria prior to the Great Oxidation Event from the 2.52 Ga Gamohaan Formation of South Africa. *Geology* **2016**, *44*, 983–986. [CrossRef]
78. Behrensmeyer, A.K.; Kidwell, S.M. Taphonomy's contributions to paleobiology. *Paleobiology* **1985**, *11*, 105–119. [CrossRef]
79. Behrensmeyer, A.K. Taphonomic and Ecologic Information from Bone Weathering. *Paleobiology* **1978**, *4*, 150–162. [CrossRef]
80. Golubic, S.; Hofmann, H.J. Comparison of Holocene and Mid-Precambrian Entophysalidaceae (Cyanophyta) in Stromatolitic Algal Mats: Cell Division and Degradation. *J. Paleontol.* **1976**, *50*, 1074–1082.
81. Oehler, J.H. Experimental studies in Precambrian paleontology: Structural and chemical changes in blue-green algae during simulated fossilization in synthetic chert. *Geol. Soc. Am. Bull.* **1976**, *87*, 117–129. [CrossRef]
82. Hofmann, H.J. Precambrian Microflora, Belcher Islands, Canada: Significance and Systematics. *J. Paleontol.* **1976**, *50*, 1040–1073.
83. Knoll, A.H.; Golubic, S. Anatomy and taphonomy of a precambrian algal stromatolite. *Precambrian Res.* **1979**, *10*, 115–151. [CrossRef]
84. Knoll, A.H.; Barghoorn, E.S. Precambrian Eukaryotic Organisms: A Reassessment of the Evidence. *Science* **1975**, *190*, 52–54. [CrossRef]
85. Horodyski, R.J.; Bloeser, B.; Haar, S.V. Laminated algal mats from a coastal lagoon, Laguna Mormona, Baja California, Mexico. *J. Sediment. Res.* **1977**, *47*, 680–696.
86. Kowalewski, M.; Flessa, K.W.; Hallman, D.P. Ternary Taphograms: Triangular Diagrams Applied to Taphonomic Analysis. *PALAIOS* **1995**, *10*, 478–483. [CrossRef]
87. Howarth, R.J. Improved estimators of uncertainty in proportions, point-counting, and pass-fail test results. *Am. J. Sci.* **1998**, *298*, 594–607. [CrossRef]
88. Weltje, G.J. Quantitative analysis of detrital modes: Statistically rigorous confidence regions in ternary diagrams and their use in sedimentary petrology. *Earth-Sci. Rev.* **2002**, *57*, 211–253. [CrossRef]

89. Systems, C.R. Sample Size Calculator. Available online: https://www.surveysystem.com/sscalc.htm (accessed on 8 January 2018).
90. Williford, K.H. DQW2 20xt Oil 2x Red. Available online: http://gigapan.com/gigapans/52663df35ba394d3cb7110452f8ebce0 (accessed on 27 July 2015).
91. Kenkel, N.C.; Juhász-Nagy, P.; Podani, J. On sampling procedures in population and community ecology. *Vegetatio* **1989**, *83*, 195–207. [CrossRef]
92. Heslehurst, M. *The Point Quadrat Method of Vegetation Analysis: A Review*; University of Reading: Reading, UK, 1971.
93. Weaver, J.E. The Quadrat Method in Teaching Ecology. *Plant World* **1918**, *21*, 267–283.
94. Toporski, J.K.; Steele, A.; Westall, F.; Thomas-Keprta, K.L.; McKay, D.S. The simulated silicification of bacteria-New clues to the modes and timing of bacterial preservation and implications for the search for extraterrestrial microfossils. *Astrobiology* **2002**, *2*, 1–26. [CrossRef]
95. Lazzeri, M.; Mauri, F. First-Principles Calculation of Vibrational Raman Spectra in Large Systems: Signature of Small Rings in Crystalline SiO_2. *Phys. Rev. Lett.* **2003**, *90*, 036401. [CrossRef] [PubMed]
96. Wacey, D. Techniques for Investigating Early Life on Earth. In *Early Life on Earth: A Practical Guide*; Spinger: Dordrecht, The Netherlands, 2009; pp. 87–123.
97. Schopf, J.W.; Kudryavtsev, A.B.; Czaja, A.D.; Tripathi, A.B. Evidence of Archean life: Stromatolites and microfossils. *Precambrian Res.* **2007**, *158*, 141–155. [CrossRef]
98. Williford, K.H.; Ushikubo, T.; Schopf, J.W.; Lepot, K.; Kitajima, K.; Valley, J.W. Preservation and detection of microstructural and taxonomic correlations in the carbon isotopic compositions of individual Precambrian microfossils. *Geochim. Et Cosmochim. Acta* **2013**, *104*, 165–182. [CrossRef]
99. Wacey, D. In situ Morphologic, Elemental and Isotopic Analysis of Archean Life. In *Evolution of Archean Crust and Early Life*; Dilek, Y., Furnes, H., Eds.; Springer: Dordrecht, The Netherlands, 2014; pp. 351–365.
100. Peng, X.T.; Guo, Z.X.; House, C.H.; Chen, S.; Ta, K.W. SIMS and NanoSIMS analyses of well-preserved microfossils imply oxygen-producing photosynthesis in the Mesoproterozoic anoxic ocean. *Chem. Geol.* **2016**, *441*, 24–34. [CrossRef]
101. R Reid, R.P.; Visscher, P.T.; Decho, A.W.; Stolz, J.F.; Bebout, B.M.; Dupraz, C.; Macintyre, I.G.; Paerl, H.W.; Pinckney, J.L.; Prufert-Bebout, L.; et al. The role of microbes in accretion, lamination and early lithification of modern marine stromatolites. *Nature* **2000**, *406*, 989. [CrossRef]
102. Jorgensen, B.B.; Revsbech, N.P.; Cohen, Y. Photosynthesis and structure of benthic microbial mats: Microelectrode and SEM studies of four cyanobacterial communities1. *Limnol. Oceanogr.* **1983**, *28*, 1075–1093. [CrossRef]
103. Stal, L.J. *Microbial Mats in Coastal Environments*; Springer: Berlin/Heidelberg, Germany, 1994; pp. 21–32.
104. Altermann, W.; Kazmierczak, J. Archean microfossils: A reappraisal of early life on Earth. *Res. Microbiol.* **2003**, *154*, 611–617. [CrossRef] [PubMed]
105. Schopf, J.W. Precambrian paleobiology: Problems and perspectives. *Annu. Rev. Earth Planet. Sci.* **1975**, *3*, 213–249. [CrossRef]
106. Bartley, J.; Knoll, A.; Grotzinger, J.P.; Sergeev, V. *Lithification and Fabric Genesis in Precipitated Stromatolites and Associated Peritidal Carbonates*; Mesoproterozoic Billyakh Group: Siberia, Russia, 2000; Volume 67.
107. Francis, S.; Barghoorn, E.S.; Margulis, L. On the experimental silicification of microorganisms. III. Implications of the preservation of the green prokaryotic alga prochloron and other coccoids for interpretation of the microbial fossil record. *Precambrian Res.* **1978**, *7*, 377–383. [CrossRef]
108. Decho, A.W. Microbial biofilms in intertidal systems: An overview. *Cont. Shelf Res.* **2000**, *20*, 1257–1273. [CrossRef]
109. Krylov, I.; Orleanskii, V.; Tikhomirova, N. Chertification: Secular Preparations. *Priroda* **1989**, *4*, 73–78.
110. Decho, A.W. Overview of biopolymer-induced mineralization: What goes on in biofilms? *Ecol. Eng.* **2010**, *36*, 137–144. [CrossRef]
111. Heaney, P.J. A proposed mechanism for the growth of chalcedony. *Contr. Mineral. Petrol.* **1993**, *115*, 66–74. [CrossRef]
112. Ortega-Calvo, J.J.; Hernandez-Marine, M.; Saiz-Jimenez, C. Biodeterioration of building materials by cyanobacteria and algae. *Int. Biodeterior.* **1991**, *28*, 165–185. [CrossRef]
113. Sergeev, V.N.; Gerasimenko, L.M.; Zavarzin, G.A. The Proterozoic History and Present State of Cyanobacteria. *Microbiology* **2002**, *71*, 623–637. [CrossRef]

114. Knoll, A.H. Exceptional Preservation of Photosynthetic Organisms in Silicified Carbonates and Silicified Peats. *Philos. Trans. R. Soc. B Biol. Sci.* **1985**, *311*, 111–122. [CrossRef]
115. Wacey, D.; Gleeson, D.; Kilburn, M.R. Microbialite taphonomy and biogenicity: New insights from NanoSIMS. *Geobiology* **2010**, *8*, 403–416. [CrossRef] [PubMed]